Studying precipitation processes in WRF with Goddard bulk microphysics in comparison with other microphysical schemes

W.-K. Tao[1], J. J. Shi[1,2], S. S. Chen[3], S. Lang[1,4], S.-Y. Hong[5], G. Thompson[6], C. Peters-Lidard[7], A. Hou[8], S. Braun[1], and J. Simpson[1]

[1]*Laboratory for Atmospheres*
NASA Goddard Space Flight Center
Greenbelt, Maryland

[2]*Science Applications International Corporation*
Beltsville, Maryland

[3]*Rosentiel School of Marine and Atmospheric Science*
University of Miami
Miami, Florida

[4]*Science Systems and Applications, Inc.*
Lanham, Maryland

[5]*Department of Atmospheric Sciences and Global Environment Laboratory*
Yonsei University
Seoul, South Korea

[6]*National Center for Atmospheric Research (NCAR)*
Boulder, Colorado

[7]*Hydrological Sciences Branch*
NASA Goddard Space Flight Center
Greenbelt, Maryland

[8]*Goddard Modeling Assimilation Office*
Greenbelt, MD 20771

February 6, 2009

Mon. Wea. Rev.

---

[1] *Corresponding author address: Dr. Wei-Kuo Tao, Code 613.1, NASA Goddard Space Flight Center, Greenbelt, MD 20771, Email: Wei-Kuo.Tao-1@nasa.gov*

Abstract

A Goddard bulk microphysical parameterization is implemented into the Weather Research and Forecasting (WRF) model. This bulk microphysical scheme has three different options, 2ICE (cloud ice & snow), 3ICE-graupel (cloud ice, snow & graupel) and 3ICE-hail (cloud ice, snow & hail). High-resolution model simulations are conducted to examine the impact of microphysical schemes on two different weather events: a midlatitude linear convective system and an Atlantic hurricane.

The results suggest that microphysics has a major impact on the organization and precipitation processes associated with a summer midlatitude convective line system. The Goddard 3ICE scheme with the cloud ice-snow-hail configuration agreed better with observations in terms of rainfall intensity and having a narrow convective line than did simulations with the cloud ice-snow-graupel and cloud ice-snow (i.e., 2ICE) configurations. This is because the Goddard 3ICE-hail configuration has denser precipitating ice particles (hail) with very fast fall speeds (over 10 m s^{-1}). For an Atlantic hurricane case, the Goddard microphysical scheme (with 3ICE-hail, 3ICE-graupel and 2ICE configurations) had no significant impact on the track forecast but did affect the intensity slightly.

The Goddard scheme is also compared with WRF's three other 3ICE bulk microphysical schemes: WSM6, Purdue-Lin and Thompson. For the summer midlatitude convective line system, all of the schemes resulted in simulated precipitation events that were elongated in the southwest-northeast direction in qualitative agreement with the observed feature. However, the Goddard 3ICE-hail and Thompson schemes were closest to the observed rainfall intensities although the Goddard scheme simulated more heavy rainfall

(over 48 mm/h). For the Atlantic hurricane case, none of the schemes had a significant impact on the track forecast; however, the simulated intensity using the Purdue-Lin scheme was much stronger than the other schemes.

The vertical distributions of model-simulated cloud species (e.g., snow) are quite sensitive to the microphysical schemes, which is an important issue for future verification against satellite retrievals. Both the Purdue-Lin and WSM6 schemes simulated very little snow compared to the other schemes for both the midlatitude convective line and hurricane case. Sensitivity tests with these two schemes showed that increasing the snow intercept, turning off the auto-conversion from snow to graupel, eliminating dry growth, and reducing the transfer processes from cloud-sized particles to precipitation-sized ice collectively resulted in a net increase in those schemes' snow amounts.

1. Introduction

Advances in computing power allow atmospheric prediction models to be run at progressively finer scales of resolution, using increasingly more sophisticated physical parameterizations and numerical methods. The representation of cloud microphysical processes is a key component of these models. Over the past decade both research and operational numerical weather prediction (NWP) models [i.e., the Fifth-generation National Center for Atmospheric Research (NCAR)/Penn State University Mesoscale Model (MM5), the National Centers for Environmental Prediction (NCEP) Eta, and the Weather Research and Forecasting Model (WRF)] have started using more complex microphysical schemes that were originally developed for high-resolution cloud-resolving models (CRMs). CRMs, which are run at horizontal resolutions on the order of 1-2 km or finer, can simulate explicitly complex dynamical and microphysical processes associated with deep, precipitating atmospheric convection. Chen *et al.* (2007) showed the importance of high-resolution in fully coupled air-sea models for hurricane prediction. A recent report to the United States Weather Research Program (USWRP) Science Steering Committee specifically calls for the replacement of implicit cumulus parameterization schemes with explicit bulk schemes in NWP as part of a community effort to improve quantitative precipitation forecasts (QPF, Fritsch and Carbone 2002).

There is no doubt that cloud microphysics play an important role in non-hydrostatic high-resolution simulations as evidenced by the extensive amount of research devoted to the development and improvement of cloud microphysical schemes and their application to the study of precipitation processes, hurricanes and other severe weather events over the past two and a half decades (see Table 1). Many different approaches have been used to examine

the impact of microphysics on precipitation processes associated with convective systems[1]. For example, ice phase schemes were developed in the 80's (Lin *et al.* 1983; Cotton *et al.* 1982, 1986; Rutledge and Hobbs 1984), and the impact of those ice processes on precipitation processes associated with deep convection were investigated (Yoshizaki 1986; Nicholls 1987; Fovell and Ogura 1988; Tao and Simpson 1989; and others). The results suggested that the propagation speed and cold outflow structure were similar between runs with and without ice-phase processes. This is because evaporative cooling and the vertical shear of the horizontal wind in the lower troposphere largely determine the outflow structure. However, ice phase microphysical processes are crucial for developing a realistic stratiform structure and precipitation statistics. The sensitivity of the different types of microphysical schemes and processes on precipitation was also investigated (i.e., McCumber *et al.* 1991; Ferrier *et al.* 1995; Wu *et al.* 1999; Tao *et al. 2003a;* and others). Those results indicated that the use of three ice classes is superior to using just two and that for tropical cumuli, the optimal mix of bulk ice hydrometeors is cloud ice, snow and graupel (i.e., McCumber *et al.* 1991). Ice microphysical processes also play an important role in the long-term simulation of cloud and cloud-radiative properties (i.e., Wu *et al.* 1999; Zeng *et al.* 2008). Additionally, water budgets and process diagrams (see Fig. 7 in Tao *et al.* 1991 and Fig. 10 in Colle and Zeng 2004) were analyzed to determine the dominant cloud and precipitation processes (i.e., Fovell and Ogura 1988; Tao *et al.* 1991; Colle and Zeng 2004; and Colle *et al.* 2005). For example, Fovell and Ogura (1988) found that the melting of hail was the primary source of rain for a long lasting mid-latitude squall line. Tao *et al.* (1990) showed that the dominant microphysical processes were quite different between the convective and stratiform regions and between the mature and decaying stages. Condensation, collection (accretion) of cloud

[1] The effects of aerosols (see a brief review by Tao *et al.* 2007) on microphysical (processes)

water by rain, and melting of graupel dominated in the convective region, while deposition, evaporation, melting and accretion associated with the ice phase dominated during the mature phase of a tropical squall line. However, melting and sublimation became important during the dissipating stage in the stratiform region. Colle *et al.* (2005) determined that condensation, snow deposition, accretion of cloud water by rain and melting are important processes associated with orographic precipitation events.

Many new and improved microphysical parameterization schemes were developed in the past decade (i.e., Ferrier 1994; Meyers *et al.* 1997; Resiner *et al.* 1998; Hong *et al.* 2004; Walko *et al.* 1995; Morrison *et al.* 2005; Straka and Mansell 2005; Milbrandt and Yau 2005; Morrison and Grabowski 2008; Thompson *et al.* 2004, 2008; Dudhia *et al.* 2008 and others). These schemes range from one-moment bulk with three ice classes to one-moment bulk with multiple ice classes to two-moment two, three and four classes of ice. Different approaches have been used to examine the performance of a new scheme. One approach is to examine the sensitivity of precipitation processes to different microphysical schemes. This approach can help to identify the strength(s) and/or weakness(es) of each scheme in an effort to improve their overall performance (i.e., Ferrier *et al.* 1995; Straka and Mansell 2005; Milbrandt and Yau 2005). Idealized simulations have also been used to test new microphysical schemes by showing their behavior in a setting that is open to simpler interpretation. In addition, another approach has been to examine specific microphysical processes (i.e., turning melting/evaporation on or off, reducing the auto-conversion rate from cloud water to rain, etc.) within one particular microphysical scheme. This approach can help to identify the dominant microphysical processes within a particular scheme (i.e.,

---

schemes have also been studied.

evaporation, melting of large precipitating ice particles, etc.) responsible for determining the organization and structure of convective systems (i.e., Tao *et al.* 1995; Wang 2002; Colle *et al.* 2005; Zhu and Zhang 2006(a); and many others).

An improved Goddard bulk microphysics parameterization (Tao *et al.* 2003a; Lang *et al.* 2007) has recently been implemented into WRF (Version 2.2.1). The major objective of this paper is to test the performance of the Goddard microphysics in WRF at very high-resolution (i.e., 1 to 1.67 km). In addition, the performance of the Goddard schemes will be compared with three other 3ICE bulk microphysical schemes in WRF: WSM6, Purdue-Lin and Thompson. Numerical experiments will be performed for two different weather events, a midlatitude convective system and an Atlantic hurricane, to investigate the impact of the microphysical parameterizations on the organization, evolution, intensity and major characteristics of the vertical distribution of cloud species.

2. Brief description of microphysical schemes

2.1 Goddard microphysical scheme

The Goddard Cumulus Ensemble (GCE) model's (Tao and Simpson 1993; Tao *et al.* 2003a) one-moment bulk microphysical schemes were recently implemented into WRF. These schemes are mainly based on Lin *et al.* (1983) with additional processes from Rutledge and Hobbs (1984). However, the Goddard microphysics schemes have several modifications. First, there is an option to choose either graupel or hail as the third class of ice (McCumber *et al.* 1991). Graupel has a relatively low density and a high intercept value (i.e., more numerous but smaller particles). In contrast, hail has a relative high density and a low

intercept value (i.e., fewer but larger particles). These differences can affect not only the description of the hydrometeor population and formation of the anvil and stratiform region but also the relative importance of specific microphysical, dynamical, radiative processes. Second, a new saturation technique (Tao *et al.* 1989) was added. This saturation technique is basically designed to ensure that super saturation (sub-saturation) cannot exist at a grid point that is clear (cloudy). The saturation scheme is one of the last microphysical processes to be computed. It is only done prior to evaluating evaporation of rain and deposition or sublimation of snow/graupel/hail. Third, all microphysical processes that do not involve melting, evaporation or sublimation (i.e., transfer rates from one type of hydrometeor to another) are calculated based on one thermodynamic state. This ensures that all of these processes are treated equally. The opposite approach is to have one particular process calculated first modifying the temperature and water vapor content (i.e., through latent heat release) before the next process is computed. Fourth, the sum of all sink processes associated with one species will not exceed its mass. This ensures that the water budget will be balanced in the microphysical calculations[2].

In addition to the two different 3ICE schemes (i.e., cloud ice, snow and graupel or cloud ice, snow and hail) that were implemented into WRF, the Goddard microphysics has two options. The first one is equivalent to a two-ice (2ICE) scheme having only cloud ice and snow. This option may be needed for coarse resolution simulations (i.e., horizontal grid sizes > 5 km). The two-class ice scheme could also be applied for winter and frontal convection. The second option is for warm rain only (i.e., cloud water and rain). Recently, the Goddard 3ICE schemes were modified to reduce over-estimated and unrealistic amounts

[2] The above Goddard microphysical scheme has been implemented into the MM5 and ARPS.

of cloud water and graupel in the stratiform region (Tao *et al.* 2003a; Lang *et al.* 2007). Various assumptions associated with the saturation technique were also revisited and examined (Tao *et al.* 2003a). These modifications are briefly described in Appendix A. In addition, transfer processes between all water species are also presented in Appendix A.

2.2 Brief description of three other microphysical schemes currently in WRF

Currently, WRF has three different one-moment bulk microphysical parameterizations each having the same five classes of hydrometeors: cloud water, rain, cloud ice, snow, and graupel. Except for Thompson *et al.* (2004, 2007), in all of the schemes the parameterized production terms are basically based on Lin *et al.* (1983) and Rutledge and Hobbs (1984) with relatively minor modifications. The most significant changes for the WSM6 and Thompson schemes are briefly mentioned below.

The WRF-Single-Moment 6-Class Microphysics (WSM6) scheme (Hong and Lim 2006) has the same five classes of hydrometeors as the Purdue-Lin scheme but with the revised ice microphysics proposed by Hong *et al.* (2004). The most distinguishing features of Hong *et al.* (2004) are: (1) practically representing ice microphysical processes by assuming the ice nuclei number concentration is a function of temperature; (2) a new assumption that the ice crystal number concentrations are a function of the amount of ice, and (3) cloud ice sedimentation. All related ice processes are changed accordingly. The saturation adjustments are based on Tao *et al.* (2003a) and separately treat the ice and water saturation processes. Hong *et al.* (2004) showed that significant improvements were made in high cloud amount, surface precipitation, and large-scale mean temperature through better representation of the ice-radiation feedback. A detailed description of the WSM6 scheme

including all the source/sink terms and the computational procedures are given in Hong and Lim (2006)[3].

The Thompson *et al.* (2008) scheme was designed to improve the prediction of freezing drizzle events for aircraft safety. Like the other schemes, this scheme has the same five classes of hydrometeors plus a prognostic ice number concentration. Whereas the previous version of WRF (v2.1) used the Thompson *et al.* (2004) code, which was primarily based on Reisner *et al.* (1998), this research utilized an entirely new Thompson *et al.* (2008) scheme found in WRF v2.2 that dramatically differs from the Lin *et al.* (1983)-based schemes. Most importantly, none of the intercept parameters are constant and all species assume a generalized gamma distribution instead of the purely exponential distribution. The intercept parameter for rain is diagnosed from the rain mixing ratio and/or from equivalent melted snow/graupel diameter relationships. The snow intercept parameter depends on both temperature and snow water content to match observations by Field *et al.* (2005). The graupel intercept parameter depends on its mixing ratio and, as such, allows the graupel category to mimic both graupel and hail. In conditions of light to moderate updrafts, smaller graupel particles (mostly from rimed snow) dominate with a terminal velocity relation closer to snow than hail. However, in relatively strong updrafts, the intercept parameter significantly decreases and the resulting terminal velocity is similar to observations for hail. Additional improvements, such as the treatment of auto-conversion and hydrometeor collision/collection, can be found in Thompson *et al.* (2008).

3. Model set-up and cases

[3] Note that in WRF (V3.0) the WSM6 scheme has a new combined terminal velocity for snow and graupel (Dudhia *et al.* 2008).

To examine the generality and applicability of the microphysical schemes, two different types of precipitation systems, a midlatitude convective system and an Atlantic hurricane (Fig. 1), were selected to test the performance of the Goddard microphysical scheme with its different options (i.e., 2ICE and both 3ICE versions). For comparison, simulations for the same case studies using WRF2.2 and the other three microphysical schemes (i.e., Purdue-Lin, WSM6 and Thompson) are also presented.

3.1 A midlatitude mesoscale convective system case

The International H2O project (IHOP_2002) was conducted over southern Kansas, Oklahoma, and northern Texas for six weeks during May and June of 2002 (13 May to 25 June 2002). Its focus was to obtain atmospheric water vapor profiles and relate them to convection initiation (CI), atmospheric boundary layer development (ABL) and quantitative precipitation forecasting (QPF). A detailed summary of the physical processes (i.e., mesoscale convergence lines and gust fronts) associated with convective storm initiation and evolution for IHOP cases can be found in Wilson and Robert (2006). The case selected is a linear convective system (see Fig. 1a) that occurred between 1200 UTC 12 and 1200 UTC 13 June. The event fell on a major IHOP study day with there being a small-scale low-pressure center located in the Oklahoma Panhandle before the development of the convective bands. The convective bands were initiated mainly via the interaction a dry line and an outflow boundary left behind from an earlier squall line (Wilson and Robert 2006). Scattered strong storms started growing by 2100 UTC 12 June and then organized into a strong squall line by 0000 UTC 13 June (upper panel of Fig. 1a). At that time, there were two major rain bands oriented from northeast to southwest, which stretched from southeast Kansas through the

eastern part of the Oklahoma Panhandle and into the Texas Panhandle. By 0300 UTC 13 June, the linear convective system had advanced into central Oklahoma and was continuing to move southeast. Although the line had been quite strong with a substantial trailing stratiform area (i.e., middle panel of Fig. 1a), it started weakening around 0600 UTC (bottom panel in Fig. 1a), dissipated quickly after 0900 UTC and was gone by 1200 UTC as it moved into Arkansas. Despite the system's short life span, maximum accumulated rainfall reached 100 mm at some locations over the 18-hour time period.

Multiple nested domains were constructed with grid resolutions of 9, 3 and 1 km, with corresponding numbers of grid points 301 x 202 x 31, 481 x 352 x 31, and 541 x 466 x 31, respectively (Fig. 2). Time steps of 30, 10 and 3.333 seconds were used in these nested grids, respectively. The coarse domain covers almost two thirds of the entire contiguous US. The finest domain covers the entire IHOP region and the immediate vicinity. The model was initialized from NOAA/NCEP global analyses (1.0^{o} by 1.0^{o}). Time-varying lateral boundary conditions were provided at 6-h intervals. The model was integrated from 0000 UTC 12 June to 1200 UTC 13 June 2002.

The Kain-Fritsch (1990, 1993) cumulus parameterization scheme was used for the coarse 9 km grid mesh. In the 3 and 1 km grid domain, the Kain-Fritsch parameterization scheme was turned off. The WRF atmospheric radiation model includes longwave and shortwave parameterizations that interact with the atmosphere. The shortwave scheme uses a broadband two-stream (upward and downward fluxes) approach for the radiative flux calculations (Dudhia 1989). The longwave scheme is based on Mlawer *et al.* (1997) and is a spectral-band scheme using the correlated-k method. The planetary boundary layer

parameterization employed the Mellor-Yamada-Janjic[4] (Mellor and Yamada 1992) Level 2 turbulence closure model through the full range of atmospheric turbulent regimes. The surface heat and moisture fluxes (from both ocean and land) were computed from similarity theory (Monin and Obukhov 1954). The land surface model is based on Chen and Dudhia (2001) and consists of a 4-layer soil temperature and moisture model with canopy moisture and snow cover prediction. It provides sensible and latent heat fluxes to the boundary layer scheme.

3.2 An Atlantic hurricane case

Hurricane Katrina was among the most significant, costliest, and deadliest storms to ever strike the United States (Knabb *et al.* 2005). It is the sixth most intense Atlantic hurricane on record (fourth at the time of occurrence) with a minimum observed central pressure of 902 hPa (see Knabb *et al.* 2005 for more details). Figure 1b shows a Tropical Rainfall Measuring Mission (TRMM) satellite overpass taken of Katrina in the central Gulf of Mexico at 0324 UTC 28 August 2005 as it was nearing Category 4 intensity. Katrina moved northward through a weakness in the subtropical ridge ahead of an advancing trough, steering it towards the north-central Gulf Coast. Maximum sustained winds dropped as the massive storm approached southeast Louisiana due to an eyewall replacement cycle, and Katrina made landfall on the 29th as a strong Category 3 storm.

Three multiple nested domains (Fig. 3) were constructed with grid resolutions of 15, 5 and 1.667 km with corresponding numbers of grid points 300 x 200 x 31, 418 x 427 x 31, and 373 x 382 x 31, respectively. The innermost domain moved with the center of the storm.

---

[4] The scheme was coded/modified by Dr. Janjic for the NCEP Eta model.

The model was integrated for 72 h from 0000 UTC 27 August to 0000 UTC 30 August 2005. A large inner domain was necessary for the Hurricane Katrina simulations because it was both an intense Category 5 hurricane and a large storm. A moving nested domain was also necessary because Hurricane Katrina moved quickly. Time steps of 30, 10 and 3.333 seconds were used in the nested grids, respectively. The model was initialized from NOAA/NCEP/GFS global analyses (1.0^{o} by 1.0^{o}). Time-varying lateral boundary conditions were provided at 6-h intervals.

The Grell-Devenyi (2002) cumulus parameterization scheme was used for the outer grid (15 km) only. For the inner two domains (5 and 1.667 km), the Grell-Devenyi parameterization scheme was turned off. The Goddard broadband two-stream (upward and downward fluxes) approach was used for the shortwave radiative flux calculations (Chou and Suarez 1999). The longwave scheme was the same used for the MCS simulations based on Mlawer *et al.* (1997). Likewise, the planetary boundary layer parameterization and the surface heat and moisture fluxes (from both ocean and land) follow the MCS case. The present WRF simulations of Katrina are not coupled to an ocean model.

4. Results

4.1 *The 12 June IHOP Case*

Figures 4, 5 and 6 show the WRF-simulated radar reflectivity from six different microphysical schemes. Generally speaking, WRF produced the right distribution of precipitation for this IHOP case despite using different microphysical schemes. For example, in all of the runs the main precipitation event is elongated in the southwest-

northeast direction and organizes into a convective line near the Texas Panhandle and northern Oklahoma as observed at 0000 UTC 13 June (Fig. 4). All of the schemes resulted in simulations wherein the main area of precipitation propagates southeastward and weakens from 0000 UTC to 0600 UTC with more light precipitation (weaker radar reflectivity, see Fig. 6). This feature also generally agrees with observations (lower panel of Fig. 1a). However, differences between the model simulations and observations are not negligible (i.e., the simulated system develops farther south and west than was observed at 0300 and 0600 UTC) and become more noticeable later in the integrations.

There are also differences between runs with different microphysical schemes. For example, the Goddard 3ICE-hail configuration resulted in a very thin and intense convective line at 0000 UTC (hour 24 into the model integration, see Fig. 4f), which seems to agree well with the observations (upper panel of Fig. 1a) compared to the two other Goddard scheme configurations. As would be expected, the simulated linear convective system is broader and less intense when using the Goddard 2ICE or 3ICE-graupel configurations. This is because snow and graupel have lower densities and hence slower fall speeds than hail. Snow or graupel forming in the convective cores can ascend to higher altitudes than hail and then be carried farther downstream from the convection before descending through the melting region. Consequently, rain (radar reflectivity) is spread over a wider area after the system reaches its mature stage; this feature could be enhanced during its decaying stage (i.e., at 0600 UTC, see Figs. 5 and 6). Snow has a slower fall speed than graupel; therefore, rain (radar reflectivity) occurs over an even larger area with the 2ICE physics (Figs. 5e and 6e) as compared to 3ICE-graupel (Figs. 5d and 6d). These results suggest that the Goddard 3ICE scheme with a cloud ice-snow-hail configuration is better for simulating intense, thin

convective lines, but the Goddard 3ICE scheme with cloud ice-snow-graupel or 2ICE with a cloud ice-snow configuration could be good for simulating the wide rain area during the decaying stage of a system.

At 0000 UTC (after 24 hours of model integration), the WSM6 and Purdue-Lin schemes are also similar to the Goddard 3ICE-hail configuration (both simulated a thin, intense convective line), but the local maximum is smaller in WSM6. Consequently, a broader rain area was simulated in WSM6 than in Purdue-Lin. Differences in the distribution of accompanying precipitation due to the reduced local maxima were found to originate from the ice-phase microphysics of Hong *et al.* (2004) as demonstrated by Hong *et al.* (2009). The model results also showed that the Purdue-Lin scheme (Figs. 4c, 5c and 6c) and Goddard 3ICE-hail configuration (Figs. 4f, 5f and 6f) are similar except that the Purdue-Lin scheme did not produce as wide of a rain area as the Goddard 3ICE-hail configuration. This could be caused by the fact that the Purdue-Lin scheme produced more rain but less snow than the Goddard 3ICE-hail configuration (see discussion later). The Thompson scheme (Fig. 4a) also led to a thin convective line at 00UTC. In addition, the Thompson scheme simulated more trailing stratiform precipitation than the other 3ICE configurations while the Purdue-Lin and 3ICE-hail simulated the least.

After 27 and 30 hours of model integration (0300 UTC and 0600 UTC), an intense rain (high radar reflectivity) area is still present along the leading edge of the system in all of the runs. Also, in all of the 3ICE runs (i.e., Thompson, Purdue-Lin, WSM6, Goddard 3ICE-graupel and 3ICE-hail), intense rain (high radar reflectivity) was simulated along the southern edge of the system in good agreement with observations. The Thompson scheme produced a broader area of light rain than the other 3ICE schemes but not as much as the

2ICE scheme (Figs. 5e and 6e). With its slower fall speed, the large amount of snow simulated in the 2ICE scheme produces a large area of light precipitation.

Both the vertical distribution of cloud species and the surface rainfall PDF are quite sensitive to the microphysical rates within the schemes. Figure 7 shows PDFs of the WRF-simulated and observed surface rainfall intensity (mm/h) and the domain average of the 24h accumulated rainfall (mm). The Goddard 2ICE configuration produced more light rain (less than 8 mm/h) but less total rainfall than the others (except 3ICE-graupel). This is because the snow particles remain in the middle and upper troposphere longer and do not fall as rapidly through the melting layer. This implies that the precipitation efficiency[5] is lower for the 2ICE simulation. The Goddard 3ICE-graupel simulation generally produced lighter and less intense precipitation than did the Goddard 3ICE-hail. The Goddard 3ICE-hail, Thompson and Purdue-Lin scheme resulted in less light precipitation (8 mm/h or less). This result seems to be in better agreement with the observations. However, the 3ICE-hail configuration simulated too much moderate and heavy rainfall (i.e., > 24 mm/h) compared to the observations and other schemes. This is because hail, which is associated with both large hydrometeor mixing ratios and high fall speeds, melts to form large rain mixing ratios and consequently high rain intensities. The Thompson and Purdue-Lin schemes also simulated more moderate and heavy rainfall. For the Thompson scheme, this is because it uses a single hydrometeor category to simulate both graupel and hail and allows partially-melted graupel to fall at the same speed as the coexisting rain below the melting level. As for the Purdue-Lin scheme, it produced very narrow and intense line convection as seen in Figs. 4, 5 and 6,

[5] Precipitation efficiency is an important physical parameter for measuring the interaction between convection and its environment. Its definition may vary (see Ferrier *et al.* 1995; Sui *et al.*

even when the density and intercept parameters were changed from hail to graupel. It also resulted in a smaller rain area than the other schemes. However, the domain average 24h-accumulated rainfall amounts from the Goddard 3ICE-hail, Thompson and Purdue-Lin scheme runs were quite similar: 10.24, 10.25, and 9.91 mm, respectively. The results from the 3ICE-graupel configuration showed both less moderate and heavy rain compared to the 3ICE-hail, Thompson and Purdue-Lin schemes. While this seems to agree better with the observations, there was also more very light rain (less than 4 mm/h) than was observed. The WSM6 scheme simulated more light rain compared to the 2ICE scheme and less heavy rain compared to the Thompson, Purdue-Lin and Goddard 3ICE-hail schemes. It also simulates less total rainfall compared to those schemes.

Fovell and Ogura (1988) showed that 3ICE with hail simulated more surface rain than did the 2ICE scheme without hail. McCumber *et al.* (1991) also showed that the 3ICE schemes (hail or graupel) simulated more surface rain than the 2ICE. The increase varied from 11 to 15 percent. Both studies were based on 2D models with single sounding initialization. In the present study, the Goddard 3ICE-hail, Thompson and Lin schemes (note all simulated more heavy rainfall) all simulate more (~11-13%) surface rain than the 2ICE over domain 2 (i.e., the 3 km grid) but not over domain 3 (i.e., the 1 km grid). This is because the simulated convective system is quite large and covers both domain 2 and 3.

Note that the simulated rainfall intensity (heavy or light) can be very important for surface processes (e.g., hydrological and ocean mixed layer models). The model results indicate that it still difficult to simulate both the rainfall intensity and the total rainfall

---

2008) but can be taken to mean the ratio of the surface rain rate to the sum of the vertically-integrated condensation and deposition rates.

accurately. More work is still needed to conduct ensemble model simulations having different microphysics (i.e., schemes with multiple ice species, multi-moments and spectral bin microphysics).

Figure 8 shows vertical profiles of the domain- and time-averaged cloud species (i.e., cloud water, rain, cloud ice, snow and graupel or hail). The Goddard 2ICE and 3ICE-graupel options both produced more cloud ice than did the Goddard 3ICE-hail option as expected (similar results were also obtained in earlier GCE model simulations, see McCumber *et al.* 1991). The Goddard 3ICE-graupel configuration produced a much larger snow profile than did the Purdue-Lin and WSM6 schemes. This is because the Goddard 3ICE-graupel parameterization assumes a larger snow intercept parameter (0.16). The snow intercept is almost one order of magnitude smaller in Purdue-Lin (0.02). This could explain the smaller amount of snow in the Purdue-Lin scheme as a lower intercept translates to larger mean sizes and greater fall speeds as well as differences in snow accretion processes. The snow intercept parameter in WSM6, however, is a function of temperature and varies from 0.02 (0 ^{o}C) to 2.43 (-40 ^{o}C). The Purdue-Lin, WSM6 and Goddard 3ICE schemes are all basically based on Lin *et al.* (1983) and Rutledge and Hobbs (1984). The modifications to the Goddard scheme described in section 2 and Appendix A might also increase snow production in the Purdue-Lin and WSM6 schemes. Additional sensitivity tests on enhanced snow production in Purdue-Lin and WSM6 are described in section 4.3.

In the Thompson scheme, snow properties are very different from the other one-moment bulk schemes. For example, its assumed snow size distribution depends on both ice water content and temperature (larger intercepts at higher altitudes). The snow is also assumed to be non-spherical and is a sum of exponential and gamma size distributions.

Constants for the snow terminal velocity are chosen to match vertically pointing radar data (see Thompson *et al.* 2008 for details). With these improvements, the simulated snow profile is expected to be large with maximum values at high altitude (Fig. 8a), which would produce a better trailing stratiform region for midlatitude squall lines. In the Thompson scheme, cloud ice is small by design because the cut-off between cloud ice and snow is extremely low. In addition, the Thompson scheme allows partially-melted graupel to fall at the same speed as the coexisting rain below the melting level, allowing precipitating ice particles to reach the lower troposphere (Fig. 8a).

Cloud model data can and often is used to infer critical cloud information that is not directly observable by satellites. The linkage between the satellite and model data usually depends on simulated brightness temperatures. As such, an accurate vertical distribution of cloud species is important for satellite retrievals (Prasad *et al.* 1995; Yeh *et al.* 1995; Lang *et al.* 2007; Olson *et al.* 2006). Unrealistic precipitation ice contents (i.e., snow and graupel), for example, can bias the simulated brightness temperatures and make it difficult to infer cloud properties from remote sensing data by linking them with synthetic values from models.

Table 2 gives the relative fraction of liquid (cloud water and rain) and solid (cloud ice, snow and graupel or hail) water contents based on time-domain averages for each scheme. The Goddard 3ICE-hail and WSM6 microphysical schemes both resulted in similar liquid (~40%) and solid (~60%) fractions. The Goddard 3ICE-graupel configuration and Thompson scheme produced higher ice fractions than 3ICE-hail and WSM6. The Goddard 2ICE option produced very little liquid while the Purdue-Lin scheme produced the most.

4.2 Hurricane Katrina

Figures 9a and b show the simulated MSLP and track, respectively, from WRF using the six different microphysical schemes/options. The simulated hurricane is stronger than was observed (i.e., the 48-hour simulated MSLP was too low) in all runs. However, this over-estimate in the intensity forecast after the first 24 hours may have resulted from an inaccurate forecast in the SSTs (or prescribed SSTs). For example, Zhu and Zhang (2006a) showed that simulated hurricane intensity could be weakened by 25 hPa by including storm-induced SST cooling. Simulated MSLP using the Goddard 2ICE configuration (16.92 hPa root mean square error or RMSE) and Thompson scheme (16.88 hPa RMSE) are the closest to the observations (from 24 to 48 hours into the forecast). Note that both of those schemes simulated less (or no) graupel compared to the other schemes[4] (Fig. 10). Minimum sea surface pressures from the Goddard 3ICE and WSM6 schemes are quite similar to each other (~19-20 hPa RMSE). The Purdue-Lin scheme, however, results in an MSLP 15-20 hPa lower than the other schemes (32 hPa RMSE). Nevertheless, the simulated temporal variation of MSLP agrees well with observations (i.e., intensification prior to landfall followed by weakening). Further analysis will be conducted to diagnose the mechanism(s) responsible for the difference in storm intensity, especially the dynamic fields (i.e., vertical velocity) as shown in Rogers *et al.* (2007).

The sensitivity tests show no significant difference (or sensitivity) in track among the different microphysical schemes. The simulated tracks are very similar prior to landfall (the first 48 hours of model integration time). The track error ranges from 76 km (Goddard 2ICE scheme) to 95 km (Thompson scheme). After landfall, the simulated tracks remain closely packed with the storm center propagating to the north-northeast. All the simulations result in

landfall farther west than was observed. The exaggerated storm intensities in the model may have affected the storm track (e.g., Fovell and Su 2007). Similar track errors were found in Shen *et al.* (2006), who used a general circulation model to assess the impact of cumulus parameterization on hurricane predictability at 0.125 degree resolution. Track errors were even larger (3~4 degree) in the WRF simulations (30 km resolution) by Rosenfeld *et al.* (2007) used to study the impact of sub-micron aerosols via warm rain suppression.

Figure 10 shows vertical profiles of the domain- and time-averaged cloud species for Hurricane Katrina. The main differences between the Goddard, Thompson, Purdue-Lin and WSM6 microphysical schemes are in the solid phase of water species at middle and upper levels. Graupel is the dominant ice species in Purdue-Lin and WSM6, while very little cloud ice is simulated by the Thompson scheme. These were also apparent in the IHOP case. Purdue-Lin and WSM6 produce very little snow (similar results were also found for another hurricane simulated by WRF) and a higher liquid fraction than the other schemes (see Table 3). In fact, all of the schemes simulate a greater proportion of liquid hydrometeors (rain processes) compared to the IHOP case. Purdue-Lin has more than a 15% increase in liquid hydrometeor fraction compared to about 8% on average for the other schemes, suggesting the Purdue-Lin scheme is more sensitive to environmental conditions than the other schemes. The Thompson scheme has a solid ice fraction similar to the Goddard 3ICE-graupel due to a relatively deep layer of high average snow contents. The Goddard 2ICE simulation has the lowest liquid fraction of all the schemes. Similar results were also found in the IHOP case.

4.3 Modification of Purdue-Lin and WSM6

Both the WSM6 and Purdue-Lin microphysical schemes simulated very little snow

compared to the Goddard and Thompson microphysical schemes for both the IHOP and Hurricane Katrina cases. There are two possible reasons for the difference in snow. One is the different intercept parameters used in the Purdue-Lin and WSM6 schemes. Another is the interaction of snow with other hydrometeor species (e.g., auto-conversion and accretion). Four additional sensitivity tests were conducted using the WSM6 and Purdue-Lin microphysical schemes. In the first two tests, the auto-conversion from snow to graupel was turned off, dry growth was eliminated, and the transfer processes from cloud-sized particles to precipitation-sized ice were reduced (Lang *et al.* 2007, see Figs. 11a and 11c for WSM6 and Purdue-Lin, respectively). In the third and fourth tests, in addition, the snow intercepts were modified from their original values to 0.16 (the value in the Goddard scheme and without the temperature dependency in WSM6, see Figs. 11b and 11d for WSM6 and Purdue-Lin, respectively). The sensitivity tests were performed for the IHOP case.

Figure 11 shows vertical profiles of the domain- and 24-h time-averaged ice species (cloud ice, snow and graupel) from the sensitivity tests using the modified WSM6 and Purdue-Lin microphysical schemes. These modifications do have an impact on snow as evidenced by the increased snow amounts for both schemes. For the Purdue-Lin scheme, the amount of snow increased significantly; for the WSM6 scheme, however, the increase in snow was much more modest without increasing the snow intercept parameter. Changing the snow intercept parameter enhanced snow amounts in both schemes (compare the snow profiles shown in Figs. 11a and b, and 11c and d). These sensitivity tests suggest that the snow intercept parameter and the transfer processes can both impact snow amounts.

Even though they were increased, the snow contents from these sensitivity tests are still smaller than the Goddard 3ICE-graupel simulation (Fig. 8d). In addition, the level of

maximum snow differs from the Thompson scheme (Fig. 8a). The level of maximum high-density ice (graupel/hail), however, is about 500 hPa in both the sensitivity tests and in the original Purdue-Lin, WSM6, Thompson and Goddard 3ICE-graupel runs. Nevertheless, more light precipitation (or radar reflectivity) over a larger area is simulated due to the increased snow amounts in both sensitivity tests (see Fig. 12). Also note that their results are quite similar to those from the Goddard 3ICE-graupel scheme (Fig. 4d).

Additional tests will be required to fully explain the differences between the schemes. For example, a simple method was proposed for the WSM6 scheme (Dudhia *et al.* 2008) to alleviate the problem of species separation by revising the paradigm that a particle must be either graupel or snow, particularly in the treatment of its fall speed, and hence trajectory, thus preventing a false separation due to their relative sedimentation rates. This new improvement could allow for more snow production.

4.4 Comparison with Previous Modeling Studies

Table 1 lists the different models, model configurations (resolution and vertical layers), and cases employed in previous high resolution cloud numerical modeling studies of precipitation processes. Similar information for the current study is shown for comparison.

(a) Hurricane cases

Only a limited number of studies have investigated microphysics in tropical cyclones and hurricanes using high-resolution (i.e., 1 – 5 km) numerical models. For example, Lord *et al.* (1984) and Willoughby *et al.* (1994) examined the impact of cloud microphysics on tropical

cyclone structure and intensity using a two-dimensional non-hydrostatic model. Their results suggested that ice processes are important for simulating tropical cyclone evolution, intensity, and structure. Including the ice case resulted in more realistic downdrafts and convective rings compared to using warm-rain only. Lord *et al.* (1984) and Willoughby *et al.* (1994) also suggested the importance of mesoscale organization on hurricane growth and structure. The mesoscale organization (especially the mesoscale downdrafts) was mainly initiated and maintained by cooling and melting. Wang (2002) used a three-dimensional numerical model to examine the impact of cloud microphysics on an idealized hurricane. His results indicated that the intensification rate and final intensity are not sensitive to microphysics (with only a few hPa difference between the runs with warm-rain only, 3ICE with graupel and 3ICE with hail) due to the similarities in the vertical profiles and magnitudes of latent heat release. The vertical profiles of cloud hydrometeors (i.e., snow and rain) and horizontal distribution of rain bands can be affected by the microphysics. For example, wider rain bands are simulated using 3ICE with graupel compared to those using warm-rain only and 3ICE with hail.

All of the above modeling studies involving microphysics and tropical cyclones were for idealized cases. Yang and Ching (2005) conducted sensitivity tests for a typhoon case (Typhoon Toraji 2001) with different microphysical schemes. Their results indicated that the track and intensity are not very sensitive to the microphysical scheme. Their results also indicated that the Goddard scheme (Tao and Simpson 1993) produced the best track while warm rain-only produced the lowest central pressure. Zhu and Zhang (2006b) investigated the sensitivity of Hurricane Bonnie (1998) to specific microphysical processes (i.e., evaporation and the melting of large precipitating ice particles). Their results indicated that

varying the cloud microphysics produces little sensitivity in hurricane track, except for the case without ice processes. However, variations in cloud microphysics were found to have a significant impact on the simulated hurricane intensity and inner core structure. Their sensitivity tests were based on one specific microphysical scheme (i.e., the Goddard scheme, Tao and Simpson 1993) whereas the sensitivity tests in this study are conducted using a variety of microphysical schemes. Li and Pu (2008) used WRF to examine the effect of cloud microphysics (i.e., warm rain only, Purdue-Lin, and WSM6) on the rapid intensification of a hurricane (Emily 2005). Their results showed that the difference in MSLP could be up to 29 hPa. On the other hand, the simulated track was not sensitive at all to the microphysical schemes with ice processes. The microphysical scheme without ice produced the earliest and quickest intensification as well as the strongest hurricane among all the simulated cases.

The simulations presented in this study have similarities and differences compared to the previous modeling studies. For example, the current simulations, Yang and Ching (2005) and Li and Pu (2008) all show that warm rain only produces the quickest intensification and the strongest hurricanes for the first 24 h of integration. These results are also in agreement with idealized simulations (Wang 2002; Lord *et al.* 1984). The dominant liquid phase in the Purdue-Lin scheme (Table 3) could explain the lower MSLP compared to the other ice schemes. In addition, the current study as well as Yang and Ching (2005), Zhu and Zhang (2006b) and Li and Pu (2008) all show that the simulated track is not sensitive to the ice microphysical scheme. Li and Pu (2008) indicated that the WSM5 (2ICE) scheme produced the weakest intensity compared to other 3ICE schemes. In this study, however, the Purdue-Lin scheme produced the strongest hurricane after 24 hours of integration and was still 20

hPa stronger than the others after 48 hours of integration. Note that all of the ice microphysical schemes produced weak hurricanes compared to the observations in Li and Pu (2008). On the other hand, all of the schemes over-predict intensity in this study. The differences could be attributed to differences in model set-up (i.e., grid size, initialization) and/or cases and environment.

(b) IHOP and midlatitude convective system cases

Jankov *et al.* (2005) examined the impact of using different WRF physical parameterizations on the simulated rain rate and domain rain volume for several cases (including the June 11-12 case) from IHOP. They found the highest sensitivity depended on the choice of convective parameterizations, with less sensitivity to the PBL schemes, and the least to microphysics. Jankov *et al.* (2007) also used WRF to examine the impact of microphysics, cumulus parameterization and PBL schemes on rainfall for different initial conditions for eight different IHOP events. They found the sensitivity to the physical schemes and their interactions depended on the initial conditions and that rain volume was sensitive to changes in both physical processes and initial conditions. The simulated rain rate was quite sensitive to the cumulus parameterization scheme despite different initial conditions. The main difference between the present and the Jankov *et al.* (2005, 2007) studies is the grid spacing (i.e., they used a 12 km grid size), which leads to differences in the conclusions.

Colle and Mass (2000) and Colle and Zeng (2004) examined the impact of microphysical schemes on orographic precipitation cases using MM5. Colle and Mass (2000) indicated that the more sophisticated 3ICE scheme does not guarantee a better

precipitation simulation. The simple 2ICE scheme with a cloud ice and snow configuration and fixed slope intercept had the best bias and RMS scores. Their study also suggests that the model results are more sensitive to the model configuration (i.e., number of vertical layers and horizontal resolution). Colle and Zeng (2004) showed that the temporal variation of precipitation, however, is similar in all schemes (i.e., warm rain only, 2ICE and 3ICE). All of the schemes also over-estimated the precipitation compared to observations. The current results also show that all of the schemes over-estimated the precipitation compared to observations. Together these studies suggest that the impact of microphysics may be quite different and depend on the case and model grid resolution.

5. Summary

The Goddard one-moment bulk liquid-ice microphysical scheme with three different options was implemented into WRF. The options are the 2ICE (cloud ice and snow), 3ICE-graupel (cloud ice, snow and graupel) and 3ICE-hail (cloud ice, snow and hail) configuration. These microphysical options also include rain processes with two classes of liquid phase (cloud water and rain). The Goddard bulk scheme also includes three different options for saturation adjustment. The Goddard bulk scheme's performance was tested and compared with three other WRF one-moment bulk microphysical schemes (i.e., Purdue-Lin, WSM6 and Thompson) for a midlatitude convective system and an Atlantic hurricane case. The major highlights are as follows:

- The Goddard scheme with a cloud ice-snow-hail configuration led to a better simulation of the summer midlatitude convective line system compared to the other two Goddard microphysical configurations. The 3ICE-hail option also

simulated less light precipitation and more moderate rainfall. These results seem to be in good agreement with observations. In addition, the 3ICE-hail configuration simulated a thin linear convective system that is also in good agreement with observations. On the other hand, the Goddard 2ICE and 3ICE-graupel options simulated convective systems that were broader and less intense. These results suggest that the optimal mix of cloud ice-snow-hail is appropriate for midlatitude squall systems as with previous 2D CRM studies (Fovell and Ogura 1998; Yang and Houze 1995; Tao *et al.* 1995, 1996). A more comprehensive study is needed, however. The Goddard 2ICE configuration results in more ice (i.e., snow) than all of the 3ICE schemes (Tables 1 and 2).

- The microphysical schemes did not have a major impact on hurricane track; however, they did affect the MSLP noticeably. The simulated hurricanes were consistently stronger than was observed in all of the WRF runs regardless of the microphysical schemes. Nevertheless, the simulated temporal variation (intensification rate) of MSLP agreed well with observations (i.e., intensification prior to landfall followed by weakening). The simulated hurricane is strongest prior to landfall and starts to weaken after landfall, which is in good agreement with observations. Simulated MSLP using the Goddard 2ICE configuration is the closest to the observations (from 24 to 48 hours into the forecast).
- The Thompson 3ICE scheme has more sophisticated snow properties and is different from the other one-moment bulk schemes presented here (see Thompson *et al.* 2008). It simulated less light precipitation and more moderate rainfall in very good agreement with observations for the IHOP case. Its simulated MSLP is also closer to the observations (from 24 to 48 hours into the forecast) than the

other 3ICE schemes, but similar to the Goddard 2ICE run. In addition, the Thompson scheme has a solid ice fraction similar to the Goddard 3ICE-graupel configuration but with more of it snow that is distributed over a deeper layer. One characteristic of the Thompson scheme is that it produced very little cloud ice in both the IHOP and hurricane cases, which is by design because the cut-off between cloud ice and snow is extremely low. Another characteristic of the Thompson scheme is that the simulated graupel/hail reaches much lower than the other schemes in the IHOP case because the Thompson scheme allows partially-melted graupel to fall at the same speed as the coexisting rain below the melting level.

- The Purdue-Lin and WSM6 schemes also simulated a linear convective system for the midlatitude case. The Purdue-Lin scheme resulted in an MSLP for the Katrina case that was 15-20 hPa lower than the other five schemes. One characteristic of the Purdue-Lin and WSM6 schemes is that both simulated much less snow and more rain than the other schemes for both the midlatitude convective system and the hurricane case. The vertical distribution of precipitating particles is quite important for accurate satellite rainfall and latent heating retrieval (Kummerow *et al.* 1996; Lang *et al.* 2007; and Olson *et al.* 2006).
- Sensitivity tests suggested that snow amounts could be increased by increasing the snow intercept, and/or collectively turning off the auto-conversion from snow to graupel, eliminating dry growth, and reducing the transfer processes from cloud-sized particles to precipitation-sized ice in the Purdue-Lin and WSM6 schemes. Additional tests will be required to fully explain the differences

between the schemes. For example, Hong *et al.* (2009) suggested that the major differences between the WSM6 and Purdue-Lin schemes are due to the ice-phase microphysics and the corresponding cloud-radiation feedback.

The sensitivity of the three different options of the Goddard ice microphysical scheme was only tested for two cases and comparisons with observations only focused on organization (including track and intensity) and rainfall intensity. Additional case studies to address microphysical processes, including more comprehensive microphysical sensitivity testing (e.g., turning off certain conversion processes from one cloud species to another), will be considered in future research. Finally, further sensitivity tests with the improved WSM6 scheme by Dudhia *et al.* (2008) as well as other microphysical schemes (i.e., Morrison *et al.* 2005; Li *et al.* 2009) are needed.

6. Acknowledgements

The authors thank Dr. D. Anderson at NASA headquarters for his support under the Cloud Modeling and Analysis Initiative (CMAI) program. The GCE microphysics development and improvements are mainly supported by the NASA Headquarters Atmospheric Dynamics and Thermodynamics Program and TRMM. The first author and Dr. J. Simpson are grateful to Dr. R. Kakar at NASA headquarters for his support of GCE development over the past decade. S.-Y. Hong was supported by the Korea Meteorological Administration Research and Development Program under Grant CATER 2007-4406.

Acknowledgment is also made to Dr. T. Lee at NASA headquarters, the NASA Goddard Space Flight Center and the NASA Ames Research Center for computer time used in this research.

7. References

Chen, F., and J. Dudhia, 2001: Coupling an advanced land-surface / hydrology model with the Penn State / NCAR MM5 modeling system.. Part I: Model description and implementation. *Mon. Wea. Rev.*, **129**, 569-585.

Chen, S. S., J. F. Price, W. Zhao, M. A. Donelan, and E. J. Walsh, 2007: The CBLAST-Hurricane Program and the next-generation fully coupled atmosphere-wave-ocean models for hurricane research and prediction. *Bull. Amer. Meteor. Soc*, **88**, 311-317.

Chou, M.-D., and M. J. Suarez, 1999: A shortwave radiation Parameterization for atmospheric studies. 15, NASA/TM-104606. pp40.

Colle, B. A., and C. F. Mass, 2000: The 5-9 February 1996 flooding event over the Pacific Northwest: Sensitivity studies and evulation of the MM5 precipitation forecasts. *Mon. Wea. Rev.*, **128**, 593-617.

Colle, B. A., and Y. Zeng, 2004: Bulk microphysical sensitivities within the MM5 for orographic precipitation. Part I: The Sierra 1986 event. *Mon. Wea. Rev.*, **132**, 2780–2801.

Colle, B. A., M. F. Garvert, J. B. Wolfe, C. F. Mass, and C. P. Woods, 2005: The 13-14 December 2001 IMPROVE-2 event. Part III: Simulated microphysical budgets and sensitivity studies. *J. Atmos. Sci.*, **62**, 3535-3558.

Cotton, W. R., M. A. Stephens, T. Nehrkorn, and G. J. Tripoli, 1982: The Colorado State University three-dimensional cloud-mesoscale model-1982. Part II: An ice-phase parameterization. *J. Rech. Atmos.*, **16**, 295-320.

Cotton, W. R., G. J. Tripoli, R. M. Rauber, and E. A. Mulvihill, 1986: Numerical simulation of the effect of varying ice crystal nucleation rates and aggregation processes on orographic snowfall. *J. Appl. Meteor.*, **25**, 1658-1679.

Dudhia, J., 1989: Numerical study of convection observed during the winter monsoon experiment using a mesoscale two-dimensional model, *J. Atmos. Sci.*, **46**, 3077-3107.

Dudhia, J., S.-Y. Hong, and K.-S. Lim, 2008: A new method for representing mixed-phase particle fall speeds in bulk microphysics parameterizations. *Special Issue on high-resolution cloud models, J. Meteor. Soc. Japan*, **86A**, 33-33.

Ferrier, B. S., 1994: A double-moment multiple-phase four-class bulk ice scheme. Part I: Description. *J. Atmos. Sci.*, **51**, 249-280.

Ferrier, B.S., W.-K. Tao and J. Simpson, 1995: A double-moment multiple-phase four-class bulk ice scheme. Part II: Simulations of convective storms in different large-scale environments and comparisons with other bulk parameterizations. *J. Atmos Sci.*, **52**, 1001-1033.

Field, P. R., R. J. Hogan, P. R. A. Brown, A. J. Illingworth, T. W. Choularton, and R. J. Cotton, 2005: Parameterization of ice-particle size distributions for mid-latitude stratiform cloud. *Quart. J. Roy. Meteor. Soc.*, **131**, 1997-2017.

Fovell, R. G., and Y. Ogura, 1988: Numerical simulation of a midlatitude squall line in two-dimensions. *J. Atmos. Sci.*, **45**, 3846-3879.

Fovell, R. G., and H. Su, 2007: Impact of cloud microphysics on hurricane track forecasts. *Geophysical Research Letters*, **34**, L24810, doi:10.1029/2007GL031723.

Fritsch, J. M., and R. E. Carbone, 2002: Research and development to improve quantitative precipitation forecasts in the warm season: A synopsis of the March 2002 USWRP Workshop and statement of priority recommendations. *Technical report to UEWRP Science Committee*,134pp.

Grell, G. A., and D. Devenyi, 2002: A generalized approach to parameterizing convection combining ensemble and data assimilation techniques. *Geophy. Res. Lett.*, **29**, Article 1693.

Hong, S.-Y., J. Dudhia, and S.-H. Chen, 2004: A revised approach to ice microphysical processes for the bulk parameterization of clouds and precipitation, *Mon. Wea., Rev.*, **132**, 103-120.

Hong, S.-Y., and J.-O. J. Lim, 2006: The WRF Single-Moment 6-Class Microphysics Scheme (WSM6). *J. Korean Meteor. Soc.*, **42**, 2, 129-151.

Hong, S.-Y., K.-S. Lim, J.-H. Kim, J.-O. Lim, and J. Dudhia, 2009: Sensitivity study of the cloud-resolving convective simulations with WRF using two-bulk microphysical parameterizations: Ice-phase microphysics versus sedimentation effects. *J. Appl. Meteor. Clim.*, **48**, 61-76.

Houze, R. A., Jr., S. S. Chen, W.-C. Lee, R. F. Rogers, J. A. Moore, G. J. Stossmeister, M. M. Bell, J. Cetrone, W. Zhao, and S. R. Brodzik, 2006: The hurricane rainband and intensity change experiment, *Bull. Amer. Meteor. Soc.*, **87**, 1503-1521.

Jankov, Isidora, W. A. Gallus Jr., M. Segal, B. Shaw, S. E. Koch, 2005: The impact of different WRF model physical parameterizations and their interactions on warm season MCS rainfall. *Wea. Forecasting*, **6**, 1048-1060.

Jankov, Isidora, W. A. Gallus Jr., M. Segal, B. Shaw, S. E. Koch, 2007: Influence of initial conditions on the WRF–ARW model QPF response to physical parameterization changes *Wea. Forecasting*, **22**, 501–519.

Kain, J. S., and J. M. Frirsch, 1990: A one-dimensional entraining/detraining plume model and its application in convective parameterization. *J. Atmos. Sci.*, **47**, 2784-2802.

Kain, J. S., and J. M. Frirsch, 1993: Convective parameterization for mesoscale models: The Kain-Fritsch scheme. The representation of cumulus convection in numerical models. K. A. Emanuel and D. J. Raymond, Eds., *Amer. Meteor. Soc.*, 246 pp.

Knabb, R. D., J. R. Rhome, and D. P. Brown, 2005: Tropical Cyclone Report – Hurricane Katrina – 23-30 August 2005. NHC/NOAA, 43 pp. [Available online at http://www.nhc.noaa.gov/2005atlan.shtml]

Kummerow, C., W. S. Olson, and L. Giglio, 1996: A simplified scheme for obtaining precipitation and vertical hydrometeor profiles from passive microwave sensors. IEEE Trans. *Geosci. Remote Sens.*, **34**, 1213–1232.

Lang, S., W.-K. Tao, R. Cifelli, W. Olson, J. Halverson, S. Rutledge, and J. Simpson, 2007: Improving simulations of convective system from TRMM LBA: Easterly and Westerly regimes. *J. Atmos. Sci.,* **64**, 1141-1164.

Li, X., and Z. Pu, 2008: Sensitivity of numerical simulation of early rapid intensification of hurricane Emily (2005) to cloud microphysical and planetary boundary layer parameterization. *Mon. Wea. Rev.*, (in press).

Li, X., W.-K. Tao, A. Khain, J. Simpson and D. Johnson, 2009: Sensitivity of a cloud-resolving model to bulk and explicit-bin microphysics schemes: Part I: Comparisons. *J. Atmos. Sci.*, **66**, 3-21.

Lin, Y.-L., R. D. Farley and H. D. Orville, 1983: Bulk parameterization of the snow field in a cloud model. *J. Clim. Appl. Meteor.*, **22**, 1065-1092.

Liu, Y., D.-L. Zhang, and M. K. Yau, 1997: A multiscale numerical study of Hurricane Andrew (1992). Part I: An explicit simulation. *Mon. Wea. Rev.,* **125**, 3073-3093.

Lord, S. J., H. E. Willoughby and J. M. Piotrowicz, 1984: Role of a parameterized ice-phase microphysics in an axisymmetric, non-hydrostatic tropical cyclone model. *J. Atmos. Sci.*, **41**, 2836-2848.

McCumber, M., W.-K. Tao, J. Simpson, R. Penc, and S.-T. Soong, 1991: Comparison of ice-phase microphysical parameterization schemes using numerical simulations of tropical convection. *J. Appl. Meteor.*, **30**, 985-1004.

Mellor, G. L., and T. Yamada, 1992: Development of a turbulence closure model for geophysical fluid problems, Rev. Geophys. Spaxe Phys., 20, 851-875.

Meyers M. P., R. L. Walko, J. Y. Harrington, and W. R. Cotton, 1997: New RAMS cloud microphysics. Part II: The two-moment scheme. *Atmos. Res.*, **45**, 3–39.

Milbrandt, J. A., and M. K. Yau, 2005: A multimoment bulk microphysics parameterization. Part II: A proposed three-moment closure and scheme description. *J. Atmos. Sci.*, **62**, 3065–3081.

Mlawer, E. J., S. J. Taubman, P. D. Brown, M. J. Jacono, and S. A. Clough, 1997: Radiative transfer for inhomogeneous atmosphere: RRTM, a validated correlated-k model for the longwave. *J. Geophys. Res.*, **102**(D14), 16663-16682.

Monin, A. S., and A. M. Obukhov, 1954: Basic laws of turbulent mixing in the surface layer of the atmosphere. *Contrib. Geophys. Inst. Acad. Sci.* USSR, (151), 163-187 (in Russian).

Morrison, H., J. A. Curry, and V. I. Khvorostyanov, 2005: A new double-moment microphysics parameterization for application in cloud and climate models. Part I: Description. *J. Atmos. Sci.*, **62**, 1665-1677.

Morrison, H., and W. Grabowski, 2008: A Novel Approach for Representing Ice Microphysics in Models: Description and Tests Using a Kinematic Framework. *J. Atmos. Sci.*, 65, 1528-1548.

Nicholls, M. E., 1987: A comparison of the results of a two-dimensional numerical simulation of a tropical squall line with observations. *Mon. Wea. Rev.,* **115,** 3055–3077.

Olson, W.-S., C. D. Kummerow,, S. Yang, G. W. Petty, W.-K. Tao, T. L. Bell, S. A. Braun, Y. Wang, S. E. Lang, D. E. Johnson and C. Chiu, 2006: Precipitation and latent heating distributions from satellite passive microwave radiometry Part I: Method and uncertainties. *J. Applied Meteor.*, **45**, 702-720.

Paterson, L. A., B. N. Hanstrum, N. E. Davidson, H. C. Weber, 2005: Influence of Environmental Vertical Wind Shear on the Intensity of Hurricane-Strength Tropical Cyclones in the Australia Region. *Mon. Wea. Rev.*, 133, 3644-3660.

Prasad, N., H.-Y. M. Yeh, R. F. Adler and W.-K. Tao, 1995: Infrared and microwave simulations of an intense convective system and comparison with aircraft observations, *J. Appl. Meteor.*, **34**, 153-174.

Reisner, J. R., R. M. Rasmussen, and R. T. Bruintjes, 1998: Explicit forecasting of supercooled liquid water in winter storms using the MM5 mesoscale model. *Quart. J. Roy. Meteor. Soc.*, **124**, 1071-1107.

Rogers, R., M. Black, S. S. Chen, and R. Black, 2007: Evaluating microphysical parameterization schemes for use in hurricane environments. Part I; Comparisons with observations. *J. Atmos. Sci.*, **64**, in press. (Available at http://orca.rsmas.miami.edu/~schen/publications/) .

Rosenfeld, D., A. Khain, B. Lynn, and W. L.Woodley, 2007: Simulation of hurricane response to suppression of warm rain by sub-micron aerosols. *Atmos. Chem. Phys.*, **7**, 3411–3424.

Rutledge, S.A., and P.V. Hobbs, 1984: The mesoscale and microscale structure and organization of clouds and precipitation in mid-latitude clouds. Part XII: A diagnostic modeling study of precipitation development in narrow cold frontal rainbands. *J. Atmos. Sci.*, **41**, 2949-2972.

Soong, S.-T., and Y. Ogura, 1973: A comparison between axisymmetric and slab-symmetric cumulus cloud models. *J. Atmos. Sci.*, **30**, 879-893.

Shen, B.-W., R. Atlas, O. Reale, S.-J. Lin, J.-D. Chern, J. Chang, C. Henze, and J.-L. Li, 2006: Hurricane forecasts with a global mesoscale-resolving model: Preliminary results with Hurricane Katrina (2005). *Geophys. Res. Lett.*, **33**, L13813, doi:10.1029/2006GL026143.

Straka, J. M., and E. R. Mansell, 2005: A bulk microphysics parameterization with multiple ice precipitation categories, *J. Appl. Meteor.*, **44**, 445-466.

Sui, C.-H., X. Li, K.-M. Lau, W.-K. Tao, M.-D. Chou and M.-J. Yang, 2008: Convective-radiative-mixing processes in the Tropical Ocean-Atmosphere. *Recent Progress in Atmospheric Sciences with Applications to the Asia-Pacific Region*, World Scientific Publication (in press).

Tao, W.-K., and J. Simpson, 1989: Modeling study of a tropical squall-type convective line. *J. Atmos. Sci.*, **46**, 177-202.

Tao, W.-K., J. Simpson and M. McCumber, 1989: An ice-water saturation adjustment. *Mon. Wea. Rev.*, **117**, 231-235.

Tao, W.-K., and J. Simpson, 1993: The Goddard Cumulus Ensemble Model. Part I: Model

description. *Terrestrial, Atmospheric and Oceanic Sciences,* **4**, 19-54.

Tao, W.-K., J. Scala, B. Ferrier and J. Simpson, 1995: The effects of melting processes on the development of a tropical and a midlatitude squall line, *J. Atmos. Sci.*, **52**, 1934-1948.

Tao, W.-K., J. Simpson, S. Lang, C.-H. Sui, B. Ferrier, and M.-D. Chou, 1996: Mechanisms of cloud-radiation interaction in the Tropics and mid-latitudes. *J. Atmos. Sci* ., **53**, 2624-2651.

Tao, W.-K., J. Simpson, D. Baker, S. Braun, M.-D. Chou, B. Ferrier, D. Johnson, A. Khain, S. Lang, B. Lynn, C.-L. Shie, D. Starr, C.-H. Sui, Y. Wang and P. Wetzel, 2003a: Microphysics, radiation and surface processes in the Goddard Cumulus Ensemble (GCE) model, *A Special Issue on Non-hydrostatic Mesoscale Modeling, Meteorology and Atmospheric Physics,* **82**, 97-137.

Tao, W.-K., C.-L. Shie, D. Johnson, R. Johnson, S. Braun, J. Simpson, and P. E. Ciesielski, 2003b*:* Convective Systems over South China Sea: Cloud-Resolving Model Simulations *J. Atmos. Sci.*, **60**, 2929-2956.

Thompson, G., R. M. Rasmussen, and K. Manning, 2004: Explicit forecasts of winter precipitation using an improved bulk microphysics scheme. Part I: Description and sensitivity analysis, *Mon. Wea., Rev.,* **132**, 519-542.

Thompson, G., P. R. Field, R. M. Rasmussen, and W. D. Hall, 2008: Explicit forecasts of winter precipitation using an improved bulk microphysics scheme. Part II: Implementation of a new snow parameterization. *Mon. Wea. Rev.*, (accepted).

Walko, R. L., W. R. Cotton, M. P. Meyers, and J. Y. Harrington, 1995:New RAMS cloud microphysics parameterization Part I: the single-moment scheme. *Atmos. Res*., **38**, 29-62.

Wang, Y., 2002: An explicit simulation of tropical cyclones with a triply nested movable mesh primitive equations model-TCM3. Part II: Model refinements and sensitivity to cloud microphysics parameterization. *Mon. Wea. Rev*., **130**, 3022-3036.

Wicker, L. J., and W. C. Skamarock, 2002: Time splitting methods for elastic models using forward time schemes. *Mon. Wea. Rev*., **130**, 2088-2097.

Willoughby, H. E., H.-L. Jin, S. J. Lord, and J. M. Piotrowicz, 1984: Hurricane structure and evolution as simulated by an axisymmetric non-hydrostatic numerical model. *J. Atmos. Sci.*, **41**, 1169-1186.

Wilson, J. W. and R. D. Roberts, 2006: Summary of convective storm initiation and evolution during IHOP: Observational and modeling perspective. *Mon. Wea. Rev*., **134**, 23–47.

Wu X., W. D. Hall, W. W. Grabowski, M. W. Moncrieff, W. D. Collins, and J. T. Kiehl, 1999: Long-term behavior of cloud systems in TOGA COARE and their interactions with radiative and surface processes. Part II: Effects of ice microphysics on cloud-radiation interaction. *J. Atmos. Sci.*, **56**, 3177–3195.

Yang, M.-J. and R. A Houze, Jr., 1995: Multicell squall-line structure as a manifestation of vertically trapped gravity waves. *Mon. Wea. Rev.,* **123,** 641-661.

Yang, M.-J. and L. Ching, 2005: A modeling study of Typhoon Toraji (2001): Physical parameterization sensitivity and topographic effect. *TAO*, **16**, 177-213.

Yeh, H.-Y. M., N. Prasad, R. Meneghini, W.-K. Tao and R. F. Adler, 1995: Model-based simulation of TRMM spaceborne radar observations, *J. Appl. Meteor.,* **34**, 175-197.

Yoshizaki, M., 1986: Numerical simulations of tropical squall-line clusters: Two-dimensional model. *J. Meteor. Soc. Japan,* **64,** 469–491.

Yuter, S. E., and Houze R. A. Jr., 1995: Three-dimensional kinematic and microphysical evolution of Florida cumulonimbus. Part II: Frequency distributions of vertical velocity, reflectivity, and differential reflectivity. Mon. Wea. Rev., 123, 1941–1963.

Zhang, D.-L., 1989: The effect of parameterized ice microphysics on the simulation of vortex circulation with a mesoscale hydroststic model. *Tellus*, **41A,** 132-147.

Zeng, X., W.-K. Tao, S. Lang, A. Y. Hou, M. Zhang, and J. Simpson, 2008: On the sensitivity of atmospheric ensembles to cloud microphysics in long-term cloud-resolving model simulations. *J. Meteor. Soc. Japan*, **86A**, 45-65.

Zhu, T., and D.-L. Zhang, 2006a: Numerical simulation of Hurricane Bonnie (1998). Part II: Sensitivity to varying cloud microphysical processes. *J. Atmos. Sci.*, **63**, 109-126.

Zhu, T., and D.-L. Zhang, 2006b: The impact of the storm-induced SST cooling on hurricane intensity. *Adv. Atmos. Sci.*, **23**,14-22.

Appendix A: Description of the Improved Goddard Microphysical Scheme

(a) Saturation adjustment

When supersaturated conditions are brought about, condensation or deposition is required to remove any surplus of water vapor. Likewise, evaporation or sublimation is required to balance any vapor deficit when sub-saturated conditions are made to occur in the presence of cloud. As the saturation vapor pressure is a function of temperature, and the latent heat released due to condensation, evaporation, deposition, and sublimation modifies the temperature, one approach has been to solve for the saturation adjustment iteratively. Soong and Ogura (1973), however, put forth a method that did not require iteration but for the water-phase only.

Tao *et al.* (1989) adopted the approach of Soong and Ogura (1973) and modified it to include the ice-phase. For temperatures over T_0 (0 ^{o}C), the saturation vapor mixing ratio is the saturation value over liquid water. For temperatures below T_{00}, which typically ranges from -30 to -40 ^{o}C (-35 ^{o}C is used in this paper), the saturation vapor mixing ratio is the saturation value over ice. The saturation water vapor mixing ratio between the temperature range of T_0 and T_{00} is taken to be a mass-weighted combination of water and ice saturation values depending on the amounts of cloud water and cloud ice present. Condensation/deposition or evaporation/sublimation then occurs in proportion to the temperature. Another approach is based on a method put forth by Lord *et al.* (1984), which weights the saturation vapor mixing ratio according to temperature between 0C and T_{00}. Condensation/deposition or evaporation/sublimation is then still proportional to temperature.

One other technique treats condensation and deposition or evaporation and sublimation sequentially. Saturation adjustment with respect to water is allowed first for a specified range of temperatures followed by an adjustment with respect to ice over a specified range of temperatures. The temperature is allowed to change after the water phase before the ice phase is treated. Please refer to Tao *et al.* (2003a) for the performance of these three different adjustment schemes. All three approaches are available in the Goddard microphysical schemes. In this paper, the last technique (sequential method) is selected.

These adjustment schemes will almost guarantee that the cloudy region (defined as the area which contains cloud water and/or cloud ice) is always saturated (100% relative humidity). This permits sub-saturated downdrafts with rain and hail/graupel particles but not cloud-sized particles. This feature is similar in many other microphysical schemes that apply saturation adjustment.

(b) Conversion of cloud particles to precipitation-sized ice

Lang *et al.* (2007) have simulated two types of convective cloud systems that formed in two distinctly different environments observed during the Tropical Rainfall Measuring Mission Large-Scale Biosphere–Atmosphere (TRMM LBA) experiment in Brazil. Model results showed that eliminating the dry growth of graupel in the Goddard 3ICE bulk microphysics scheme effectively reduced the unrealistic presence of high-density ice in the simulated anvil. However, comparisons with radar reflectivity data using contoured-frequency-with-altitude diagrams (CFADs, see Yuter and Houze 1995) revealed that the resulting snow contents were too large. The excessive snow was reduced primarily by lowering the

collection efficiency of cloud water by snow and resulted in further agreement with the radar observations (see Fig. 7 in Lang *et al.* 2007). The transfer of cloud-sized particles to precipitation-sized ice appears to be too efficient in the original scheme. Overall, these changes to the microphysics lead to more realistic precipitation ice contents in the model. The improved precipitation-sized ice signature in the model simulations lead to better latent heating retrievals as a result of both better convective-stratiform separation within the model as well as more physically realistic hydrometeor structures for radiance calculations. However, there appeared to be additional room for improvement in that simulated brightness temperatures showed that there was still too much precipitation-sized ice aloft. This indicates that despite the improvement, the overall transfer rate of cloud-sized particles to precipitation-sized particles was still too efficient. Lang *et al.* (2007) felt that the Bergeron process could be a contributing factor.

(c) The Bergeron process

An important process in the budget for cloud ice is the conversion of cloud ice to snow as the ice crystals grow by vapor deposition in the presence of cloud water, usually referred to as the Bergeron process and designated P_{SFI} (production of snow from ice) by Lin *et al.* (1983). The formulation generally used in the parameterization is independent of relative humidity, which causes ice to be converted to snow even when the air is sub-saturated with respect to ice. One alternative formulation is to simply multiply the original formula by a relative-humidity dependent factor so that P_{SFI} diminishes as the relative humidity approaches the ice saturation value. A second alternative formulation can be derived directly from the equation for depositional growth of cloud ice (Rutledge and Hobbs 1984) used in

the model. This formulation also causes PSFI to diminish as the relative humidity approaches the ice saturation value and is physically consistent with the parameterization for depositional growth of cloud ice. The two alternative formulations produce relatively similar results since simulated ice clouds over tropical oceans often have vapor mixing ratios near the ice saturation value so that PSFI is very small. The new formulation for P_{SFI} based on the simple relative-humidity correction factor was adopted and results in an increase in cloud-top height and a substantial increase in the cloud ice mixing ratios, particularly at upper levels in the cloud.

Table A1 shows the list of microphysical processes that parameterize the transfer between water vapor, cloud water, rain, cloud ice, snow and graupel/hail in the Goddard scheme implemented into WRF. The formula in each process can be found in Lin *et al.* (1983), Rutledge and Hobbs (1984), Tao and Simpson (1993), Tao *et al.* (2003a), and Lang *et al.* (2007).

	Cloud Water (QC)	**Rain (QR)**	**Cloud Ice (QI)**	**Snow (QS)**	**Graupel/Hail (QH)**
Condensation	CND				
Evaporation	*DD*	*ERN*			
Auto-conversion	*-PRAUT*	+PRAUT			
Accretion	*-PRACW*	+PRACW			
Deposition DEPOSITION OF QS DEPOSITION OF QG			PIDEP PINT DEP	PSDEP	
Sublimation			*-DD1*	*-PSSUB*	
Melting	PIMLT	PSMLT PGMLT	-PIMLT	*-PSMLT*	*-PGMLT*
AUTOCONVERSION OF QI TO QS			*-PSAUT*	PSAUT	
ACCRETION OF QI TO QS			*-PSACI*	PSACI	
ACCRETION OF QC BY QS (RIMING) (QSACW FOR PSMLT)	*-PSACW* *-QSACW*	QSACW		PSACW	
ACCRETION OF QI BY QR			*-PRACI*	del3* PRACI	(1-del3)* PRACI
ACCRETION OF QR OR QH BY QI		*-PIACR*		del3* PIACR	(1-del3)* PIACR
BERGERON PROCESSES FOR QS	*-PSFW*			PSFW	
BERGERON PROCESSES FOR QS			*-PSFI*	PSFI	
ACCRETION OF QS BY QH (DGACS,WGACS: DRY AND WET)				*-PGACS* *-DGACS* *-WGACS*	PGACS DGACS WGACS
ACCRETION OF QC BY QH (QGACW FOR PGMLT)	*-DGACW* *-QGACW*				DGACW QGACW
ACCRETION OF QI BY QH (WGACI FOR WET GROWTH)			*-DGACI* *-WGACI*		DGACI WGACI
ACCRETION OF QR TO QH (QGACR FOR PGMLT)		*-DGACR* *-(1-del)** *WGACR* *-del** *WGACR*			DGACR WGACR
WET GROWTH OF QH					
SHED PROCESS		QGACW		WGACR= PGWET- DGACW- WGACI- WGACS	QGACW
AUTOCONVERSION OF QS TO QH				*-PGAUT*	PGAUT
FREEZING		*-PGFR*			PGFR
ACCRETION OF QS BY QR				*-PRACS*	PRACS
ACCRETION OF QR BY QS (QSACR FOR PSMLT)		*-PSACR*		del2* PSACR	(1-del2)* PSACR
HOMOGENEOUS FREEZING OF QC TO QI (T < T00)	*-PIHOM*		PIHOM		
DEPOSITION GROWTH OF QC TO QI	*-PIDW*		PIDW		

Table 1A List of microphysical processes (abbreviation and brief description) that parameterize the transfer between water vapor, cloud water, rain, cloud ice, snow and graupel/hail in the Goddard scheme implemented into WRF. Source terms are in regular font and sink terms in italic font. The formula in each process can be found in Lin et al. (1983), Rutledge and Hobbs (1984), Tao and Simpson (1993), Tao et al. (2003a), and Lang et al. (2007). Del, del2 and del3 are 1 or 0 and depend on the value of the mixing ratio of cloud species (see Lin et al. 1983).

Figure Captions

Fig. 1 **(a)** Observed WSR-88D reflectivity at 0000 UTC (top), 0300 UTC (middle), and 0600 UTC (bottom) 13 June 2002 (Source: NOAA/NESDIS Satellite and Information Service). Note that these images are a vertical composite of the reflectivity and depict the highest reflectivity measured over each point on the Earth's surface. **(b)** The left panel shows the horizontal rain intensity pattern associated with Hurricane Katrina as observed by TRMM. Rain rates in the center of the swath are from the TRMM Precipitation Radar (PR), and those in the outer portion are from the TRMM Microwave Instrument (TMI). The rain rates are overlaid on infrared (IR) data from the TRMM Visible Infrared Scanner (VIRS). The right panel shows a 3D rendering of Hurricane Katrina constructed from TRMM PR data with a cutaway view through the eye of the storm. Tall towers are indicated in red on the isosurface. Images are courtesy of H. Pierce (NASA GSFC/SSAI).

Fig. 2 Nesting configuration used for the IHOP simulations. Horizontal resolutions for domains 1, 2, and 3, are 9, 3 and 1 km, respectively.

Fig. 3 Nesting configuration used for the Hurricane Katrina simulations. Horizontal resolutions for domains 1, 2 and 3, are 15, 5 and 1.667 km, respectively. Note that the inner domain is moved to follow the cyclone.

Fig. 4 Simulated radar reflectivity (in dBZ) using WRF with six different microphysical schemes for the IHOP case. The **(a)** Thompson, **(b)** WSM6 and **(c)** Purdue-Lin scheme are part of WRF's current options, and the **(d)** 3ICE-graupel, **(e)** 2ICE and **(f)** 3ICE-hail are the Goddard options. The reflectivities were calculated from model-simulated precipitation particles (rain, snow and graupe/hail) at the 24-hour model integration time, which corresponds to 0000 UTC 13 June 2002 (top panel of Fig. 1(a)). The results plotted are from the 2nd domain (i.e., 3-km resolution) in order to show the full aerial extent of the convective system.

Fig. 5 Same as Fig. 4 except at the 27-hour model integration time corresponding to 0300 UTC 13 June 2002 (middle panel of Fig. 1(a)).

Fig. 6 Same as Fig. 4 except at the 30-hour model integration time corresponding to 0600 UTC 13 June 2002 (bottom panel of Fig. 1(a)).

Fig. 7 PDF (probability distribution function) of WRF-simulated hourly rainfall intensity from six different microphysical schemes. The results were obtained from the 1-km domain for the period 1200 UTC 12 June to 1200 UTC 13 June 2002. The observed PDF derived from hourly MESONET rain gauge data is also shown for comparison. The small box inside the figure shows the domain average 24h-accumulated rainfall (mm).

Fig. 8 Vertical profiles of domain- and 24-hour time-average (between 0000 UTC 12 June and 0000 UTC 13 June 2002) cloud species (i.e., cloud water, rain, cloud ice, snow

and graupel/hail) for the **(a)** Thompson, **(b)** WSM6, **(c)** Purdue-Lin **(d)** 3ICE-graupel, **(e)** 2ICE and **(f)** 3ICE-hail schemes. Note that the scale in the 2ICE scheme is larger than the others.

Fig. 9 **(a)** Minimum sea level pressure (hPa) obtained from WRF forecasts of Hurricane Katrina using six different microphysical schemes: Thompson, Purdue-Lin, WSM6, 3ICE-graupel, 3ICE-hail and 2ICE from 0000 UTC 27 August to 0000 UTC 30 August 2005. The observed minimum sea level pressure (solid black line) is also shown for comparison. **(b)** shows the corresponding hurricane tracks for the data shown in (a). The best track is shown in black for comparison and was obtained from the National Hurricane Center.

Fig. 10 Same as Fig. 8 except for the Hurricane Katrina case and a 48-hour time-average (between 1200 UTC 27 August and 1200 UTC 29 August 2005).

Fig. 11 Vertical profiles of domain- and 24-hour time-averaged solid cloud species (cloud ice, snow and graupel) for the IHOP case using the modified WSM6 and Purdue-Lin schemes. Black lines represent values from the original (un-modified) WSM6 [**(a)** and **(b)**] and Purdue-Lin [**(c)** and **(d)**] schemes. Gray lines in (a) are for values from the modified WSM6 scheme (i.e., based on Lang *et al.* 2007 wherein the auto-conversion from snow to graupel was turned off along with a reduction in the transfer processes from cloud-sized particles to precipitation-sized ice) but with the WSM6 snow intercept parameter a function of air temperature, while in (b) they represent the modified WSM6 scheme but using the fixed Goddard snow intercept

parameter (0.16 cm^{-4}) in addition. The gray lines in (c) are for the modified (also based on Lang *et al.* 2007) Purdue-Lin scheme with the Purdue-Lin snow intercept parameter (0.03 cm^{-4}), while in (d) they represent the modified Purdue-Lin scheme but with the Goddard snow intercept parameter (0. 16 cm^{-4}).

Fig. 12 Simulated radar reflectivity (in dBZ) after 24 hours of model integration using WRF with the modified Purdue-Lin and WSM6 microphysical schemes for the IHOP case. The top panel is the modified Purdue-Lin scheme and the bottom panel the modified WSM6 scheme (auto-conversion from snow to graupel was turned off along with dry growth and a reduction in the transfer processes from cloud-sized particles to precipitation-sized ice).

Table Captions

Table 1 Key papers using high-resolution numerical cloud models (including those that developed new improved microphysical schemes) to study the impact of microphysical schemes on precipitation. Model type (2D or 3D), microphysical scheme (one moment or multi-moment bulk), resolution (km), number of vertical layers, time step (seconds), case and integration time (hours) are all listed. Papers with a "*" are used for comparison with the present study, papers with a "#" denote development of a new scheme, papers with a "$" modify/improve existing schemes, papers with a "&" compare different schemes, and papers with a "%" indicate process (budget) studies. TCM3 stands for the "Tropical Cyclone Model with triple nested movable mesh". Also only papers with bulk schemes are listed. MM5 stands for the Penn State/NCAR Mesoscale Model Version 5.

Table 2 Domain- and 24-h time-average accumulated liquid (warm rain) and solid (ice) water species for the IHOP case. The time-average is based on 24, hourly data outputs.

Table 3 Same as Table 2 except for Hurricane Katrina using 72, hourly data outputs.

	Model	*Microphysics*	*Resolutions Vertical Layers*	*Integration Time*	*Case*
Lin *et al.* (1983)	2D	3-ICE	200 m/95	48 min	Hail Event Montana
Cotton *et al.* (1982, 1986)	2D	3-ICE & Ni	500 m/31	5 hours	Orographic Snow
Rutledge and Hobbs (1984)	2D Kinematics	3-ICE	600 m/20	Steady State	Narrow Cold Front
Lord *et al.* (1984) *	2D axisymmetric	3-ICE vs Warm Rain	2 km/20	4.5 days	Idealized
Yoshizaki (1986)#	2D slab-symmetric	3-ICE scheme vs Warm Rain	0.5 km/32	4.5 hours	12 September GATE Squall Line
Nicholls (1987)	2D slab-symmetric	3-ICE vs Warm Rain	0.5 km/25	5 hours	12 September GATE Squall Line
Fovell and Ogura (1988)#%	2D slab-symmetric	3-ICE vs Warm Rain	1 km/31	10 hours	Mid-latitude Squall Line
Tao and Simpson (1989, 1993)#	2D and 3D	3-ICE vs Warm Rain	1 km/31	12 hours	GATE Squall Line
Tao *et al.* (1990)	2D	3-ICE	1 km/31	12 hours	GATE Squall Line
McCumber *et al.* (1991)%$	2D and 3D	3-ICE scheme (graupel vs hail, 2ICE vs 3ICE)	1 km/31	12 hours	GATE Squall Line
Wu *et al.* (1999)	2D slab-symmetric	2 ICE	3 km/52	39 days	TOGA COARE
Ferrier (1994), Ferrier *et al.* (1995)#	2D slab-symmetric	2-moment 4-ICE	1 km/31	12 hours	COHMEX, GATE Squall Line
Tao *et al.* (1995)	2D slab-symmetric	3-ICE	0.75 and 1 km/31	12 hours	EMEX, PRESTORM
Walko *et al.* (1995)#	2D	4-ICE	0.3 km/80	30 min	Idealized
Meyers *et al.* (1997)#$	2D	2-moment 4-ICE	0.5 km/80	30 min	Idealized
Straka and Mansell (2005)#	3D	10-ICE	0.5 km/30?	~2 hours	Idealized
Lang *et al.* (2007)$	3D	3-ICE	.25 to 1km /41	8 hours	LBA
Zeng *et al.* (2008)$	2D and 3D	3-ICE	1 km/41	40 days	SCSMEX, KWAJEX
Milbrandt and Yau (2005)#	1D	Three-moment	/51	50 minutes	Idealized Hail Storm
Morrison *et al.* (2005)#	Single column model	Two moments and 2-ICE	Single column model 27 layers	3 days	SHEBA FIRE-FACE
Morrison and Grabowski (2008)#	2D	Two-moment ICE	50 m/60	90 minutes	Idealized
Reisner *et al.* (1998)#	MM5 Non-hydrostatic	3-ICE and 2-moment for ICE	2.2 km/27	6 hours (2.2 km grid)	Winter Storms
Thompson *et al.* (2004)#	MM5 2D	3-ICE	10 km/39	3 hours	Idealized
Thompson *et al.* (2008)$	WRF 2D	3-ICE	10 km/39	6 hours	Idealized
Colle and Mass (2000)	MM5 Non-hydrostatic	3-ICE	1.33 km/38	96 hours	Orographic Flooding
Colle and Zeng (2004)%	2-D MM5 Non-hydrostatic	3-ICE	1.33 km/39	12 hours	Orographic
Colle *et al.* (2005)%	MM5 Non-hydrostatic	3-ICE	1.33 km/320	36 hours	IMPROVE
Yang and Ching (2005)*	MM5 Non-hydrostatic	3-ICE	6.67 km/23	2.5 days	Typhoon Toraji (2001)
Zhu and Zhang (2006b)*	MM5 Non-hydrostatic	3-ICE	4 km/24	5 days	Bonnie (1998)
Wang (2002)*	TCM3-hydrostatic	3-ICE	5 km/21	5 days	Idealized
Hong *et al.* (2004)#	WRF Non-hydrostatic	3-ICE	45 km/23	48 hours	Korean Heavy Rainfall event
Li and Pu (2008)*	WRF Non-hydrostatic	2-ICE and 3-ICE	3 km/31	1.25 days	Hurricane Emily (2005)
Jankov *et al.* (2005; 2007)*	WRF Non-hydrostatic	2-ICE and 3ICE	12 km/31	1 day	IHOP
Dudhia *et al.* (2008)***	WRF Non-hydrostatic	3-ICE	5 km/31	1.5 days	Korean Heavy Snow event
Tao *et al.* (2009) – Present study	WRF Non-hydrostatic	2-ICE and 3ICE	1 km/31 1.667 km/31	1.5 days 3 days	IHOP and Hurricane Katrina (2005)

Table 1 *Key papers using high-resolution numerical cloud models (including those that developed new improved microphysical schemes) to study the impact of microphysical schemes on precipitation. Model type (2D or 3D), microphysical scheme (one moment or multi-moment bulk), resolution (km), number of vertical layers, time step (seconds), case and integration time (hours) are all listed. Papers with a "*" are used for comparison with the present study, papers with a "#" denote development of a new scheme, papers with a "$" modify/improve existing schemes, papers with a "&" compare different schemes, and papers with a "%" indicate process (budget) studies. TCM3 stands for the "Tropical Cyclone Model with triple nested movable mesh". Also only papers with bulk schemes are listed. MM5 stands for the Penn State/NCAR Mesoscale Model Version 5.*

	3ICE-Hail	*3ICE-Graupel*	*2Ice*	*WSM6*	*Lin*	*Thompson*
Liquid hydrometeor	**37.3%**	**28.5%**	**15.5%**	**42.5%**	**48.9%**	**27.3%**
Solid Hydrometeor	**62.7%**	**71.5%**	**84.5%**	**57.5%**	**51.1%**	**72.7%**

Table 2 Domain- and 24-h time-average accumulated liquid (warm rain) and solid (ice) water species for the IHOP case. The time-average is based on 24, hourly data outputs.

	3ICE-Hail	*3ICE-Graupel*	*2Ice*	*WSM6*	*Lin*	*Thompson*
Liquid hydrometeor	**46.6%**	**36.4%**	**24.8%**	**50.4%**	**65.3%**	**34.2%**
Solid Hydrometeor	**53.4%**	**63.6%**	**75.2%**	**49.6%**	**34.7%**	**65.8%**

Table 3 Same as Table 2 except for Hurricane Katrina using 72, hourly data outputs

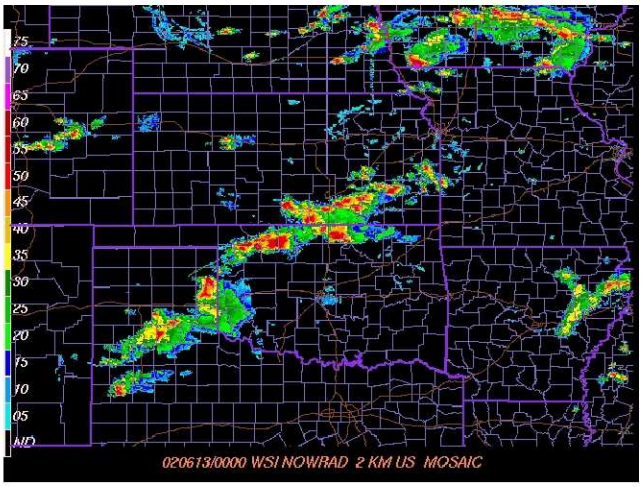

0000 UTC 6/13/2002

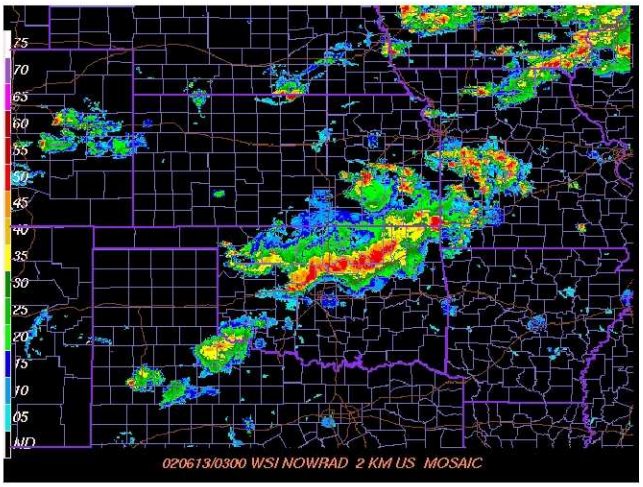

0300 UTC 6/13/2002

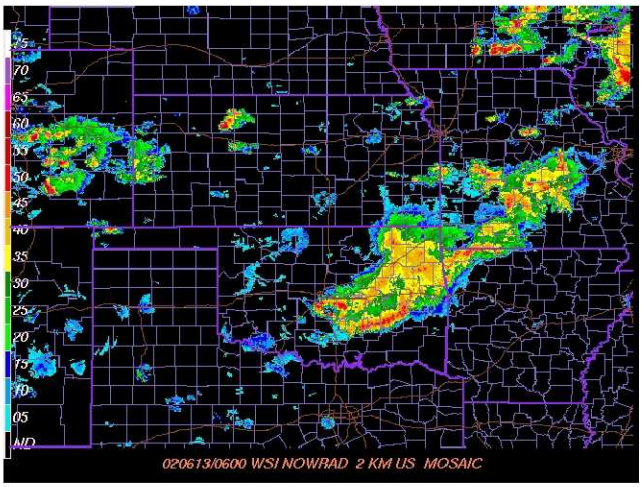

0600 UTC 6/13/2002

Fig. 1(a) Observed WSR-88D reflectivity at 0000 UTC (top), 0300 UTC (middle), and 0600 UTC (bottom) 13 June 2002 (Source: NOAA/NESDIS Satellite and Information Service). Note that these images are a vertical composite of reflectivity and depict the highest reflectivity measured over each point on the

Earth's surface.

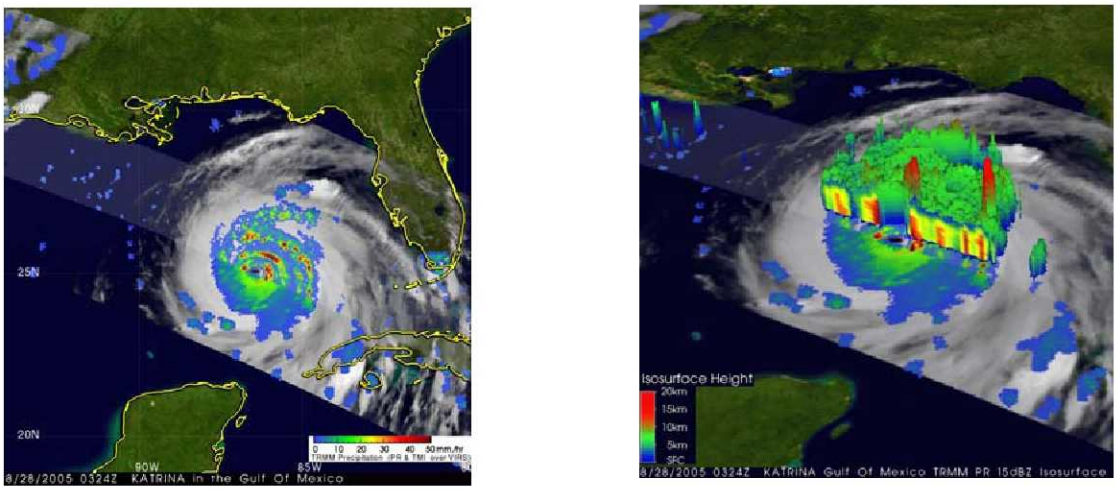

Fig. 1(b) The left panel shows the horizontal rain intensity pattern associated with Hurricane Katrina as observed by TRMM. Rain rates in the center of the swath are from the TRMM Precipitation Radar (PR), and those in the outer portion are from the TRMM Microwave Instrument (TMI). The rain rates are overlaid on infrared (IR) data from the TRMM Visible Infrared Scanner (VIRS). The right panel shows a 3D rendering of Hurricane Katrina constructed from TRMM PR data with a cutaway view through the eye of the storm. Tall towers are indicated in red on the isosurface. Images are courtesy of H. Pierce (NASA GSFC/SSAI).

.

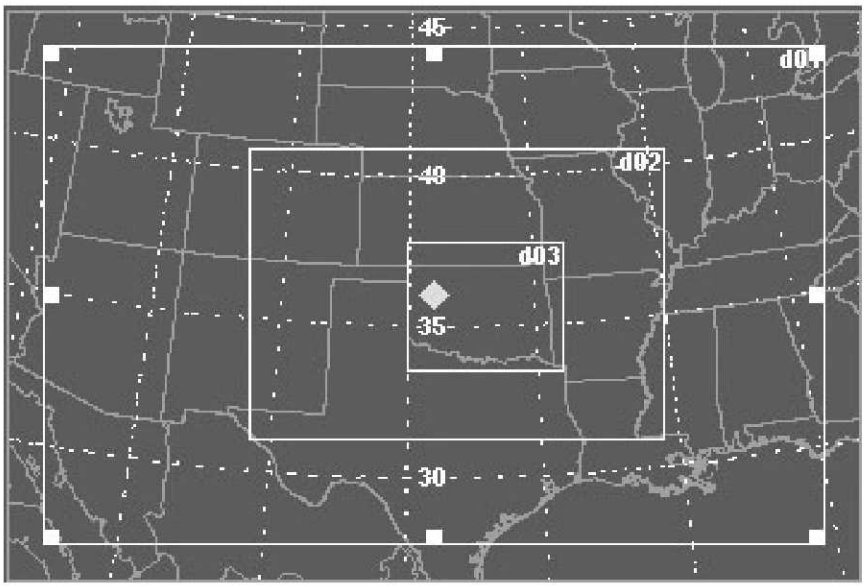

Fig. 2 Nesting configuration used for the IHOP simulations. Horizontal resolutions for domains 1, 2, and 3, are 9, 3 and 1 km, respectively.

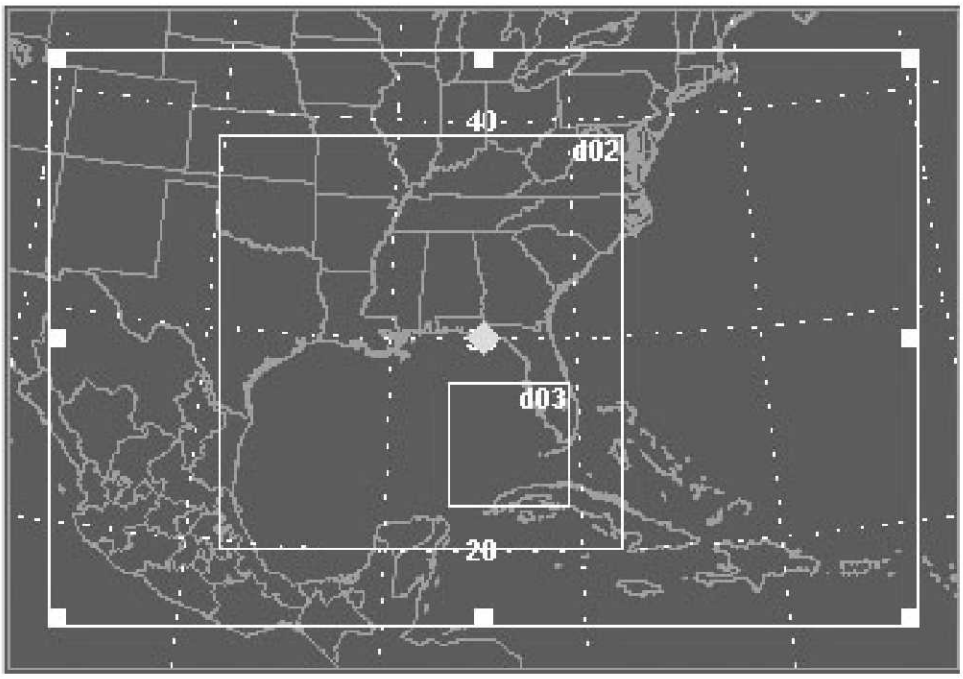

Fig. 3 *Nesting configuration used for the Hurricane Katrina simulations. Horizontal resolutions for domains 1, 2 and 3, are 15, 5 and 1.667 km, respectively. Note that the inner domain is moved to follow the cyclone.*

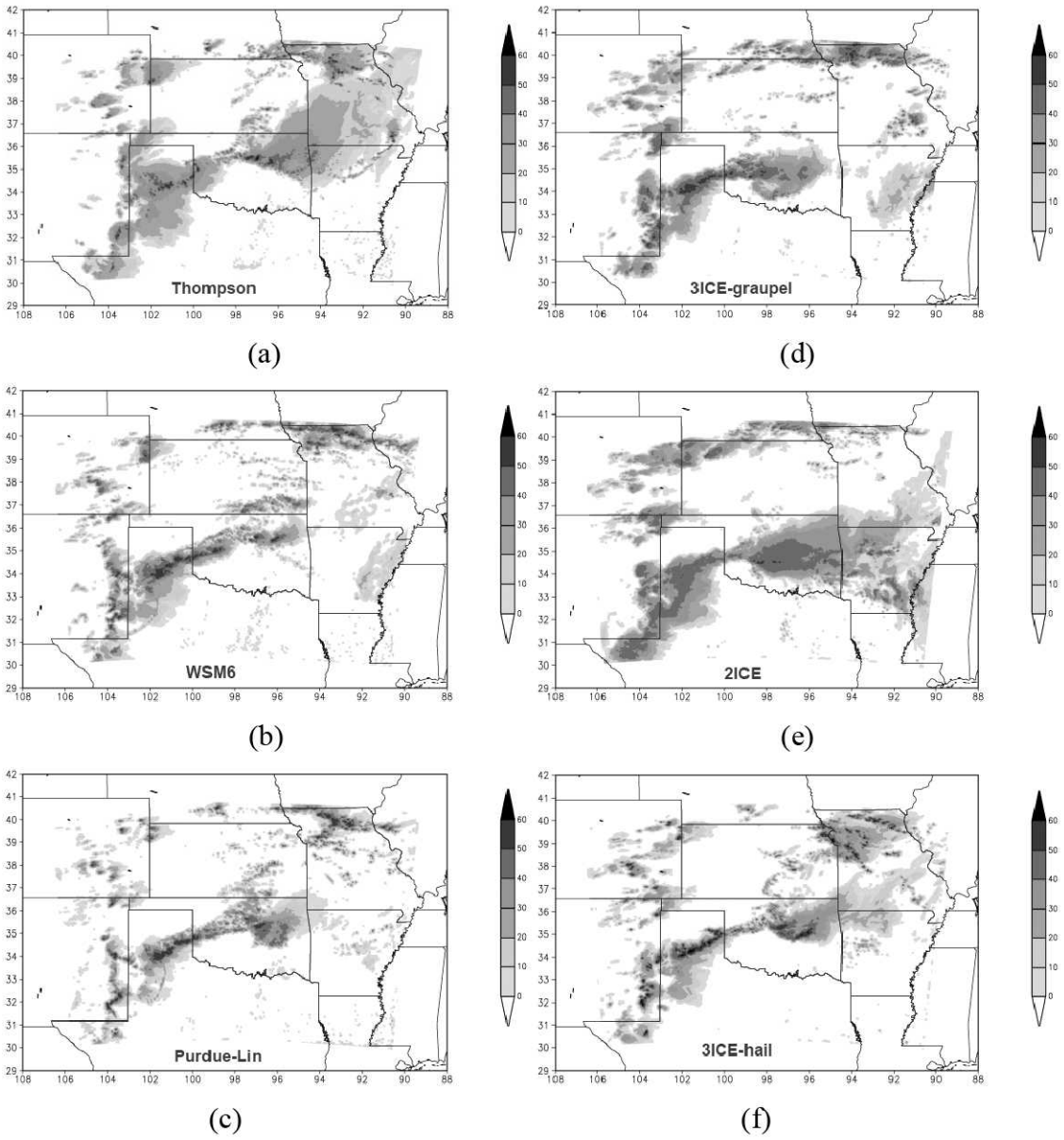

*Fig. 4 Simulated radar reflectivity (in dBZ) using WRF with six different microphysical schemes for the IHOP case. The **(a)** Thompson, **(b)** WSM6 and **(c)** Purdue-Lin scheme are part of WRF's current options, and the **(d)** 3ICE-graupel, **(e)** 2ICE and **(f)** 3ICE-hail are the Goddard options. The reflectivities were calculated from model-simulated precipitation particles (rain, snow and graupe/hail) at the 24-hour model integration time, which corresponds to 0000 UTC 13 June 2002 (top panel of Fig. 1(a)). The results plotted are from the 2nd domain (i.e., 3-km resolution) in order to show the full aerial extent of the convective system.*

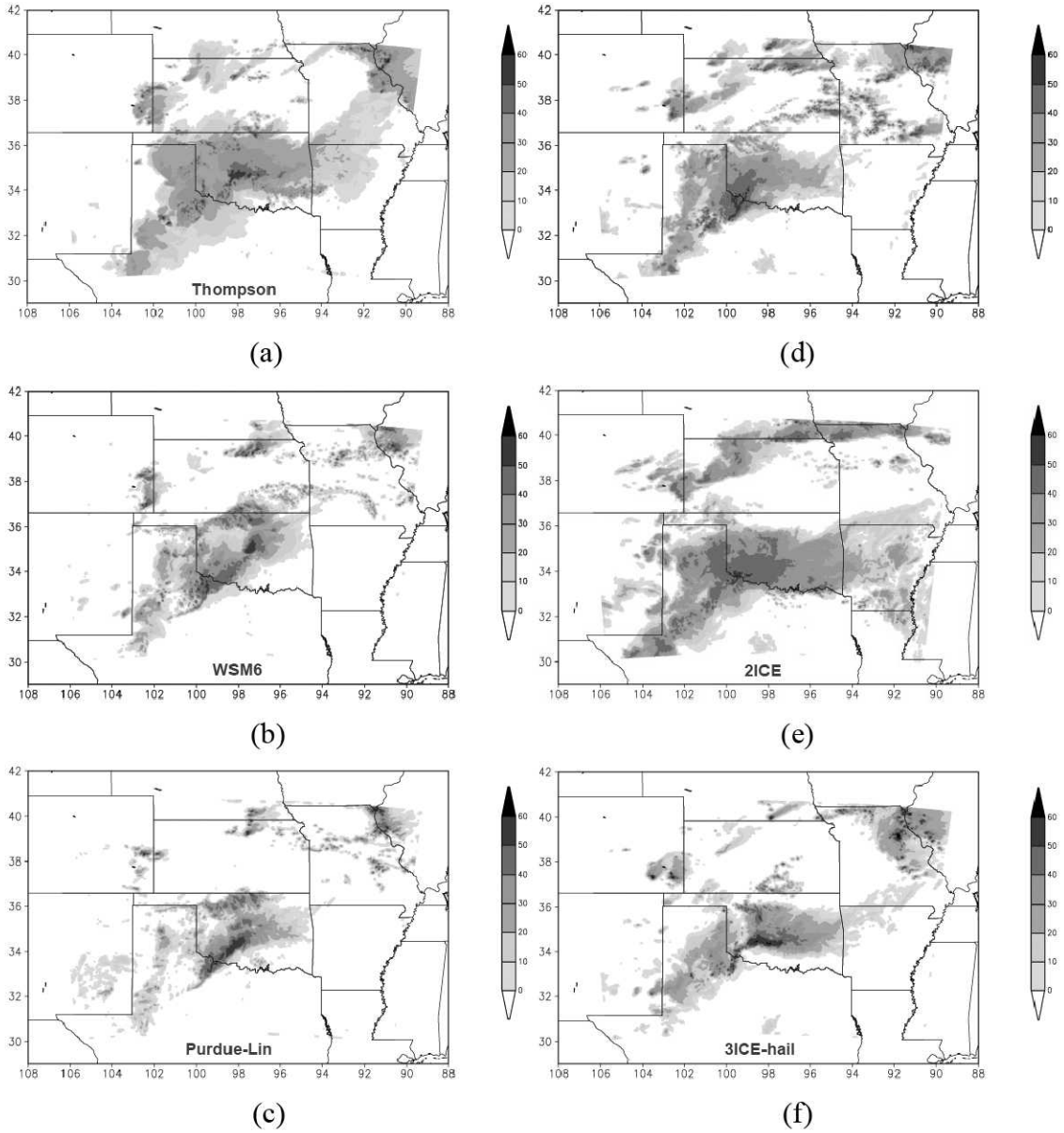

Fig. 5 Same as Fig. 4 except at the 27-hour model integration time corresponding to 0300 UTC 13 June 2002 (middle panel of Fig. 1(a)).

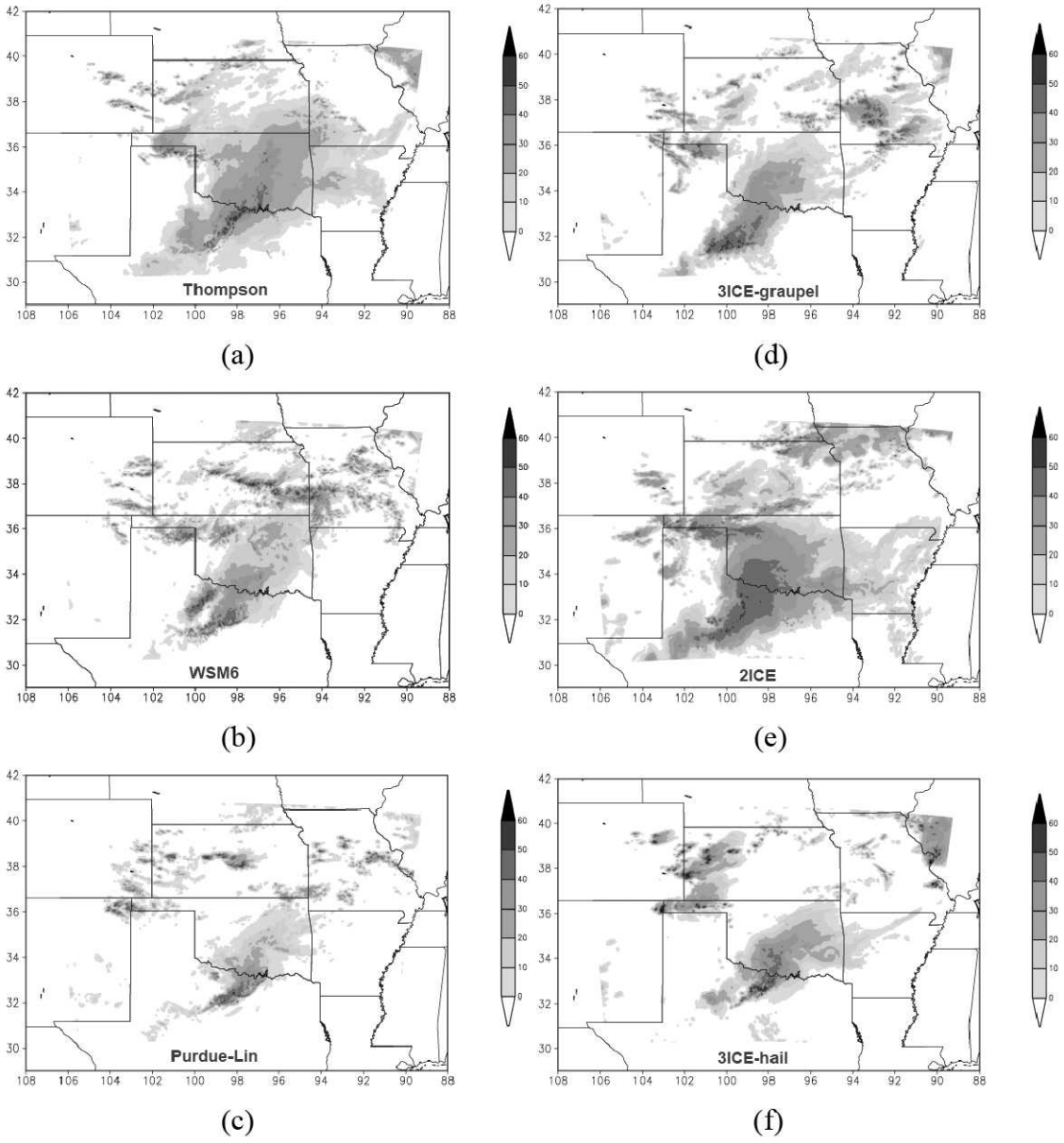

Fig. 6 Same as Fig. 4 except at the 30-hour model integration time corresponding to 0600 UTC 13 June 2002 (bottom panel of Fig. 1(a)).

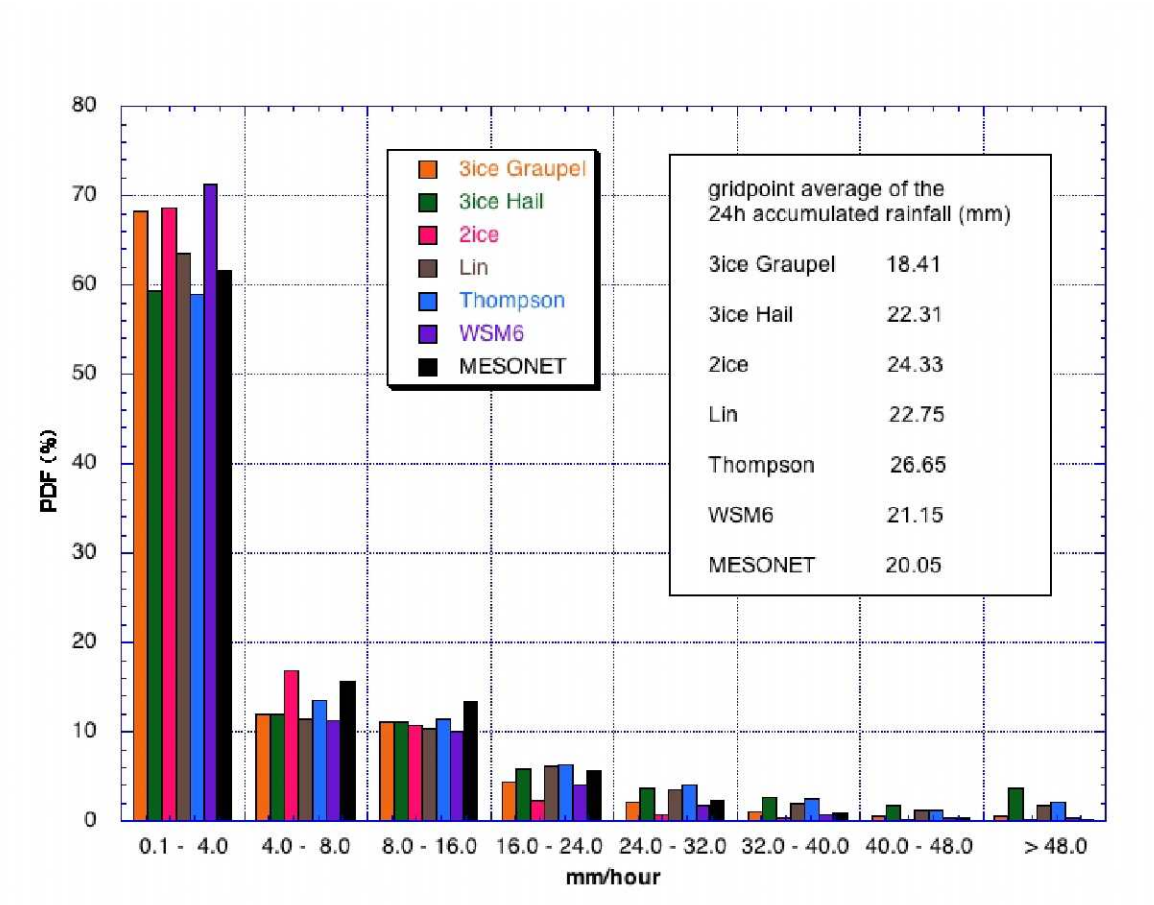

Fig. 7 *PDF (probability distribution function) of WRF-simulated hourly rainfall intensity from six different microphysical schemes. The results were obtained from the 1-km domain for the period 1200 UTC 12 June to 1200 UTC 13 June 2002. The observed PDF derived from hourly MESONET rain gauge data is also shown for comparison. The small box inside the figure shows the domain average 24h-accumulated rainfall (mm).*

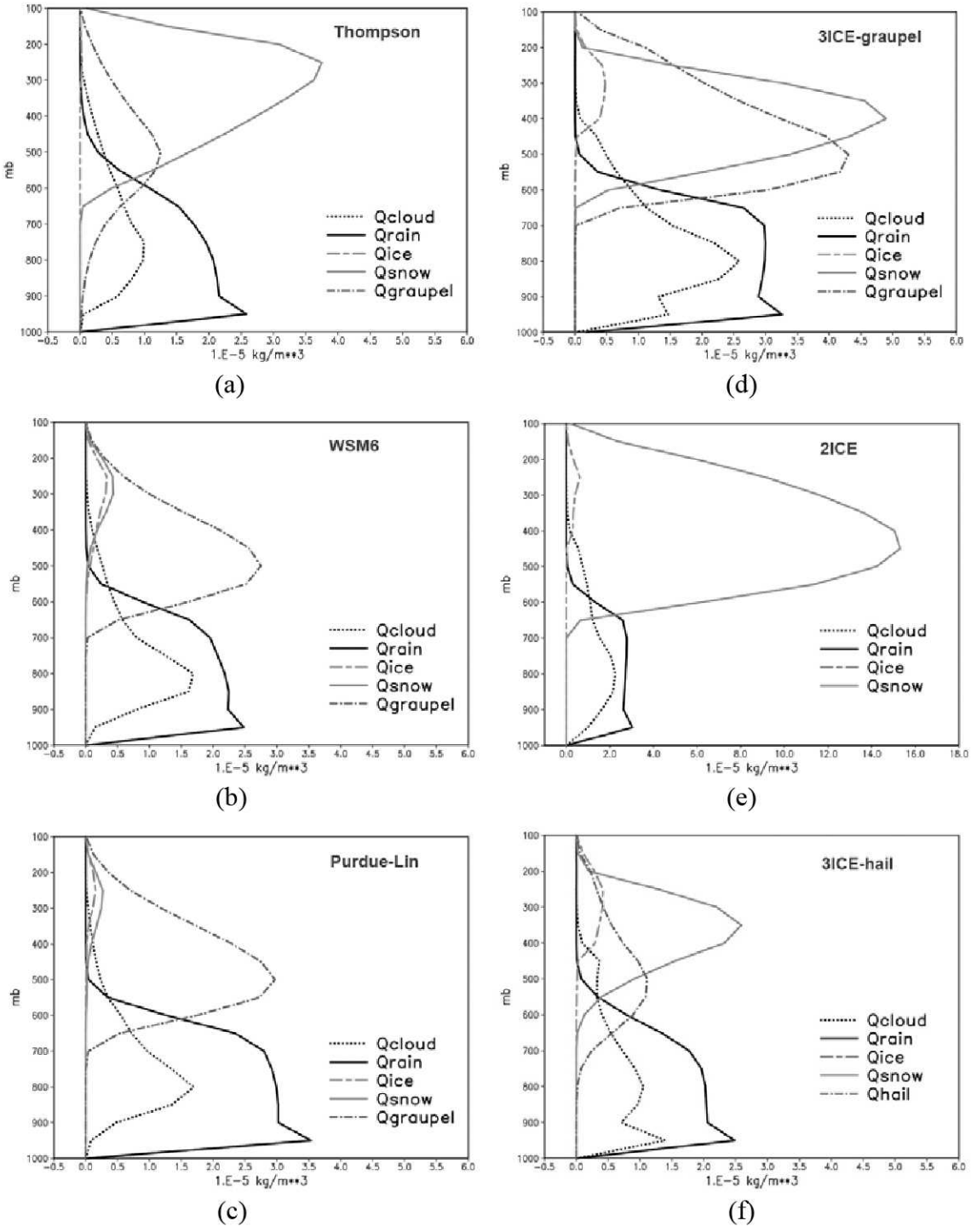

*Fig. 8 Vertical profiles of domain- and 24-hour time-average (between 0000 UTC 12 June and 0000 UTC 13 June 2002) cloud species (i.e., cloud water, rain, cloud ice, snow and graupel/hail) for the **(a)** Thompson, **(b)** WSM6, **(c)** Purdue-Lin **(d)** 3ICE-graupel, **(e)** 2ICE and **(f)** 3ICE-hail schemes. Note that the scale in the 2ICE scheme is larger than the others.*

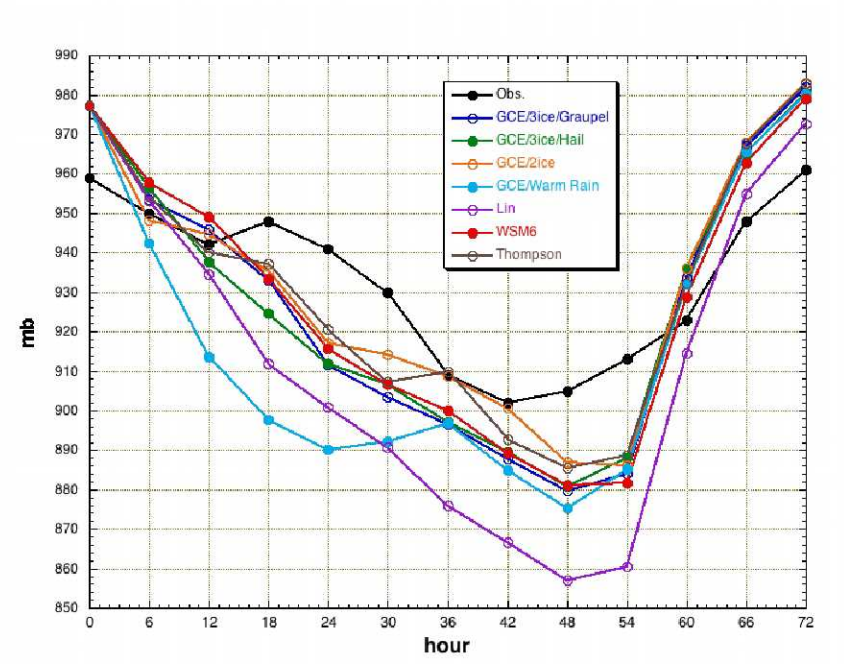

*Fig. 9(**a**) Minimum sea level pressure (hPa) obtained from WRF forecasts of Hurricane Katrina using six different microphysical schemes: Thompson, Purdue-Lin, WSM6, 3ICE-graupel, 3ICE-hail and 2ICE from 0000 UTC 27 August to 0000 UTC 30 August 2005. The observed minimum sea level pressure (solid black line) is also shown for comparison.*

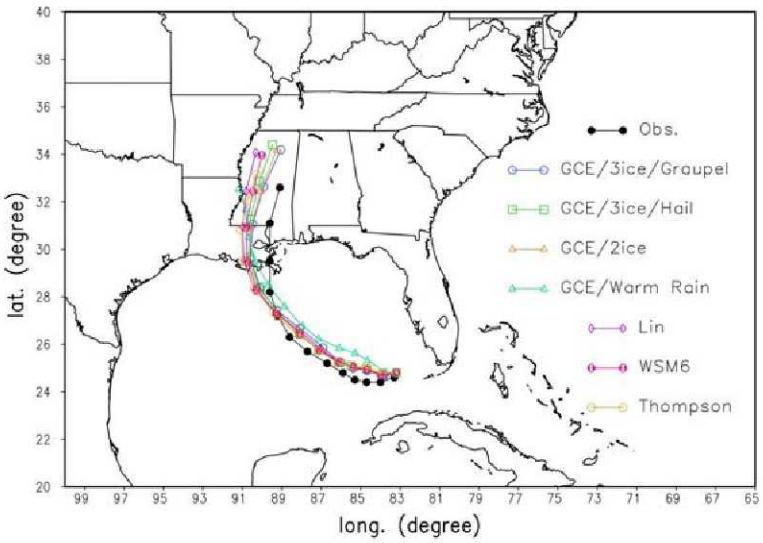

Fig. 9(b) shows the corresponding hurricane tracks for the data shown in (a). The best track is shown in black for comparison and was obtained from the National Hurricane Center.

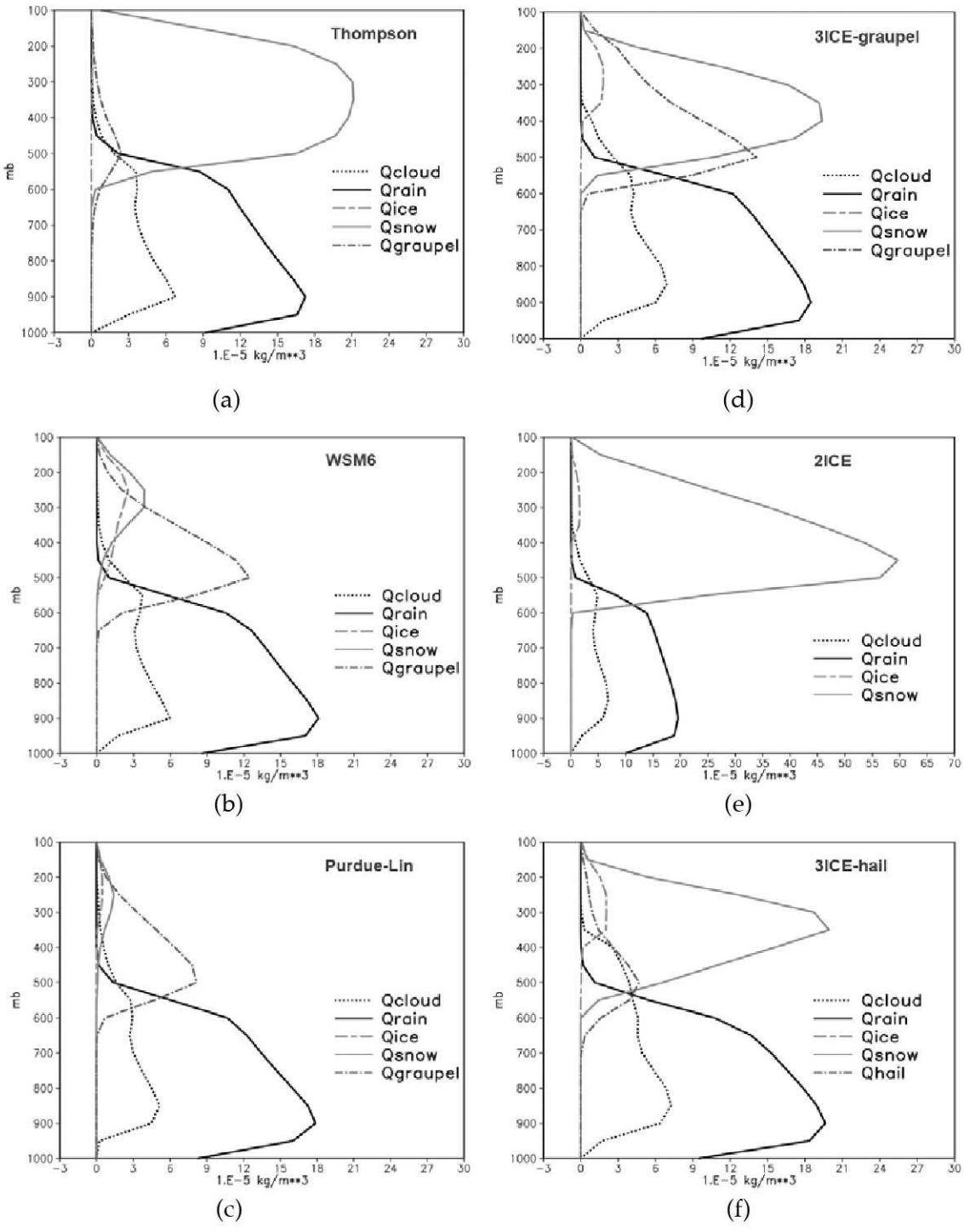

Fig. 10 Same as Fig. 8 except for the Hurricane Katrina case and a 48-hour time-average (between 1200 UTC 27 August and 1200 UTC 29 August 2005).

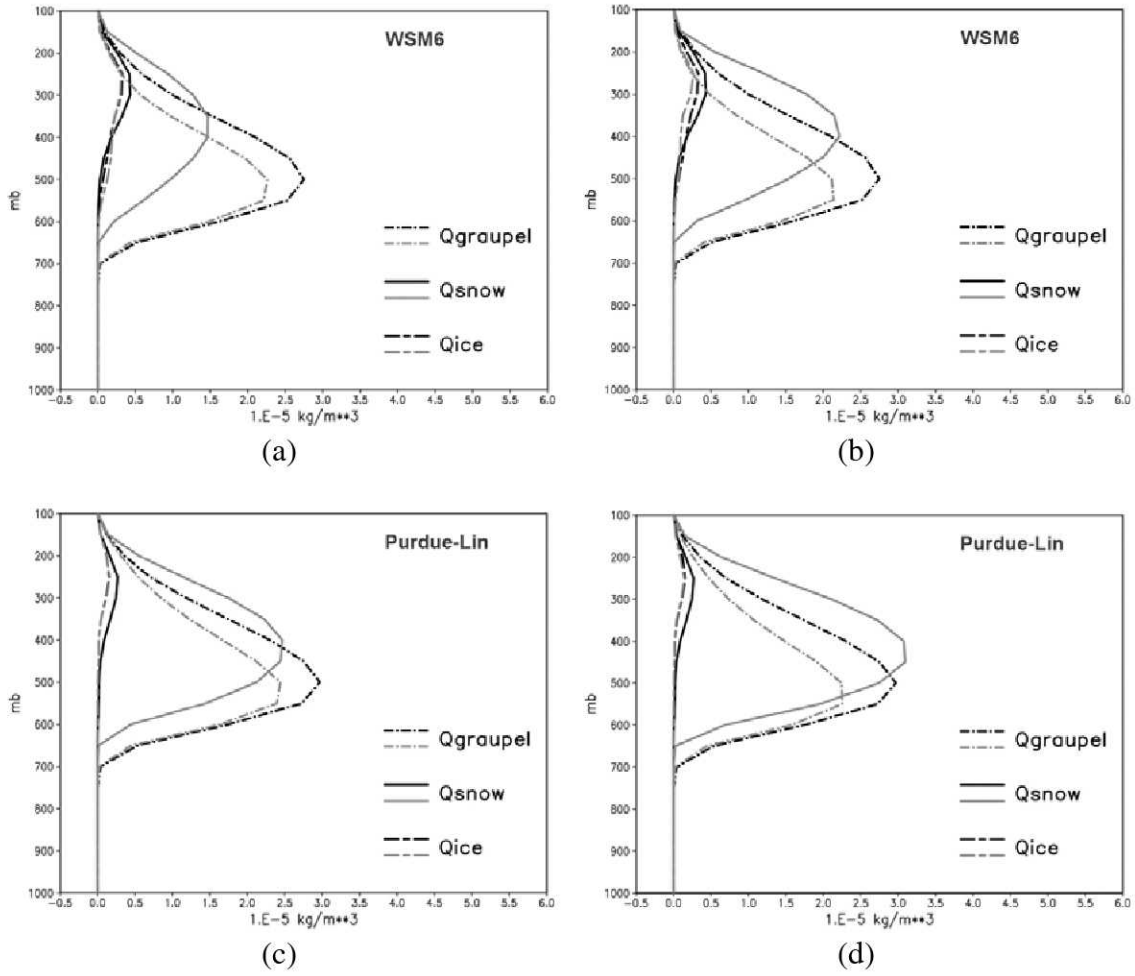

*Fig. 11 Vertical profiles of domain- and 24-hour time-averaged solid cloud species (cloud ice, snow and graupel) for the IHOP case using the modified WSM6 and Purdue-Lin schemes. Black lines represent values from the original (un-modified) WSM6 [**(a)** and **(b)**] and Purdue-Lin [**(c)** and **(d)**] schemes. Gray lines in (a) are for values from the modified WSM6 scheme (i.e., based on Lang et al. 2007 wherein the auto-conversion from snow to graupel was turned off along with a reduction in the transfer processes from cloud-sized particles to precipitation-sized ice) but with the WSM6 snow intercept parameter a function of air temperature, while in (b) they represent the modified WSM6 scheme but using the fixed Goddard snow intercept parameter (0.16 cm^{-4}) in addition. The gray lines in (c) are for the modified (also based on Lang et al. 2007) Purdue-Lin scheme with the Purdue-Lin snow intercept parameter (0.03 cm^{-4}), while in (d) they represent the modified Purdue-Lin scheme but with the Goddard snow intercept parameter (0. 16 cm^{-4}).*

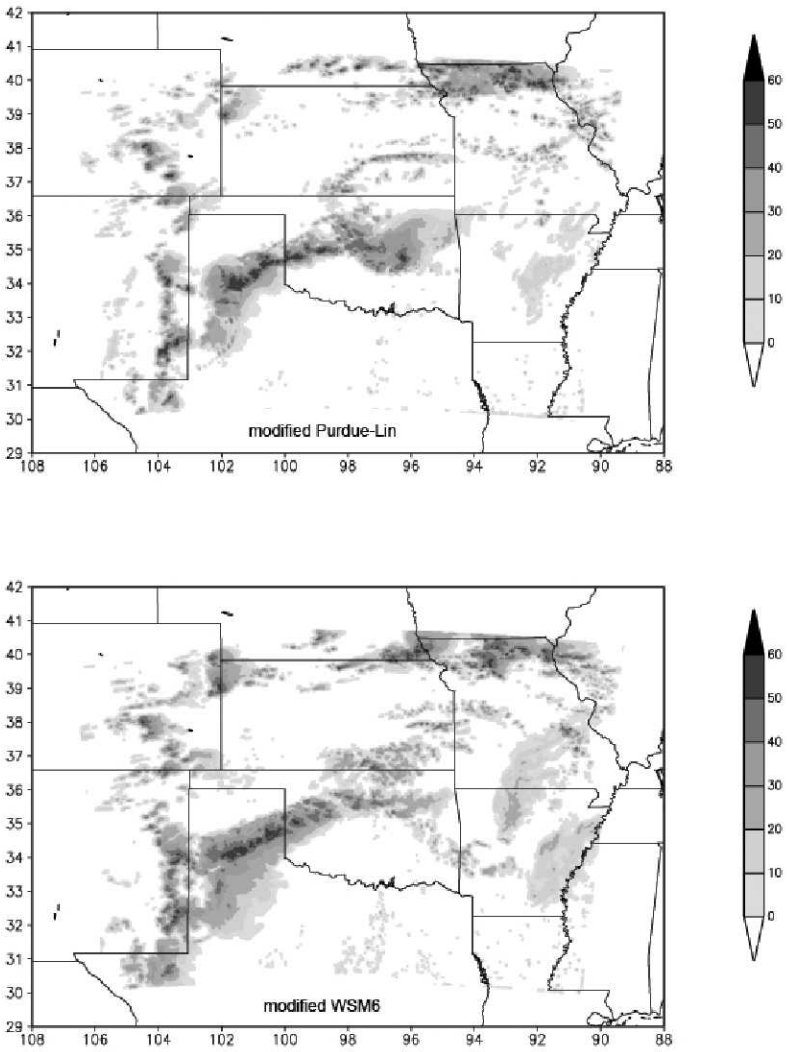

Fig. 12 Simulated radar reflectivity (in dBZ) after 24 hours of model integration using WRF with the modified Purdue-Lin and WSM6 microphysical schemes for the IHOP case. The top panel is the modified Purdue-Lin scheme and the bottom panel the modified WSM6 scheme (auto-conversion from snow to graupel was turned off along with dry growth and a reduction in the transfer processes from cloud-sized particles to precipitation-sized ice).